PCCP

Physical Chemistry Chemical Physics

This paper was published in a themed issue of *PCCP* on:

Colloidal particles at liquid interfaces

Guest Editor: Professor B. P. Binks

Please take a look at the full table of contents for this issue

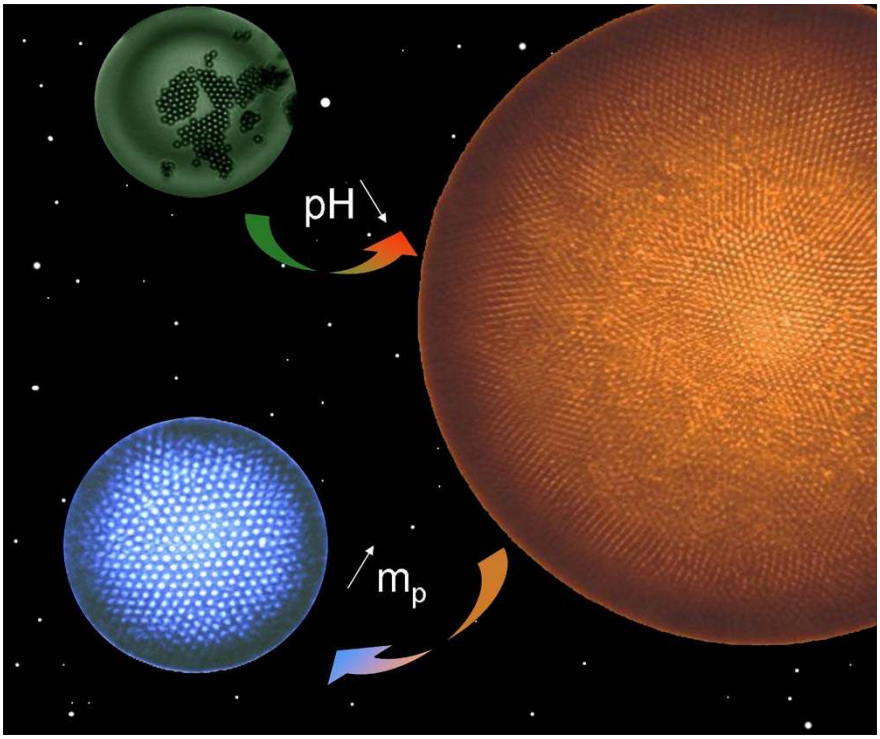

Papers in this issue include:

Stepwise interfacial self-assembly of nanoparticles *via* specific DNA pairing

Bo Wang, Miao Wang, Hao Zhang, Nelli S. Sobal, Weijun Tong, Changyou Gao, Yanguang Wang, Michael Giersig, Dayang Wang and Helmuth Möhwald, *Phys. Chem. Chem. Phys.*, 2007

DOI : 10.1039/b705094a

Water-in-carbon dioxide emulsions stabilized with hydrophobic silica particles

Stephanie S. Adkins, Dhiren Gohil, Jasper L. Dickson, Stephen E. Webber and Keith P. Johnston, *Phys. Chem. Chem. Phys.*, 2007

DOI : 10.1039/b711195a

Effect of electric-field-induced capillary attraction on the motion of particles at an oil–water interface

Mariana P. Boneva, Nikolay C. Christov, Krassimir D. Danov and Peter A. Kralchevsky, *Phys. Chem. Chem. Phys.*, 2007

DOI : 10.1039/b709123k

PCCP

Physical Chemistry Chemical Physics

www.rsc.org/pccp

Volume 10 | Number 12 | 28 March 2008 | Pages 1597–1712

SURFACTANTS

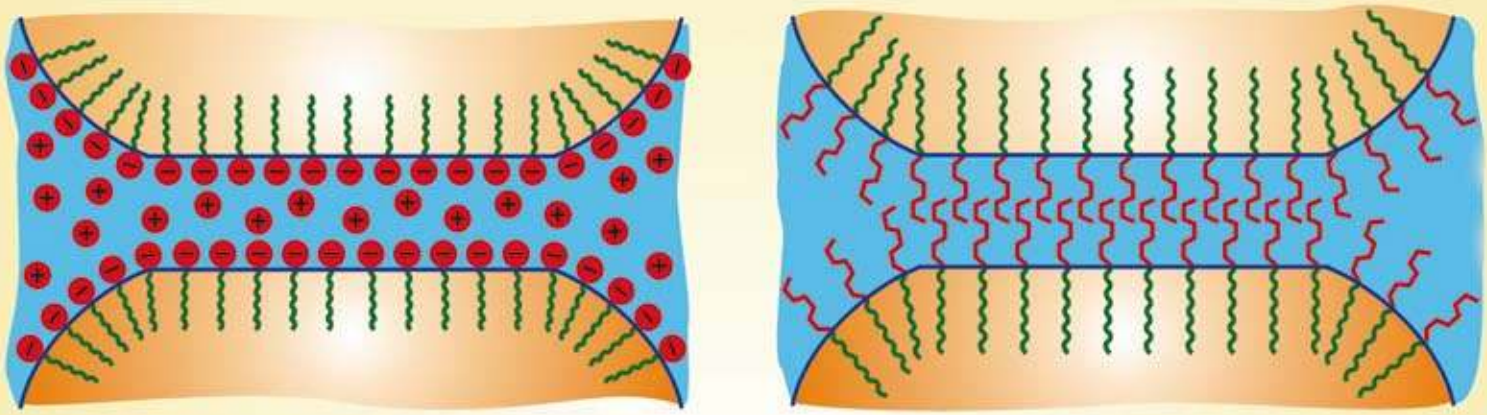

OSMOTIC STABILIZATION OF EMULSION FILMS

PARTICLES

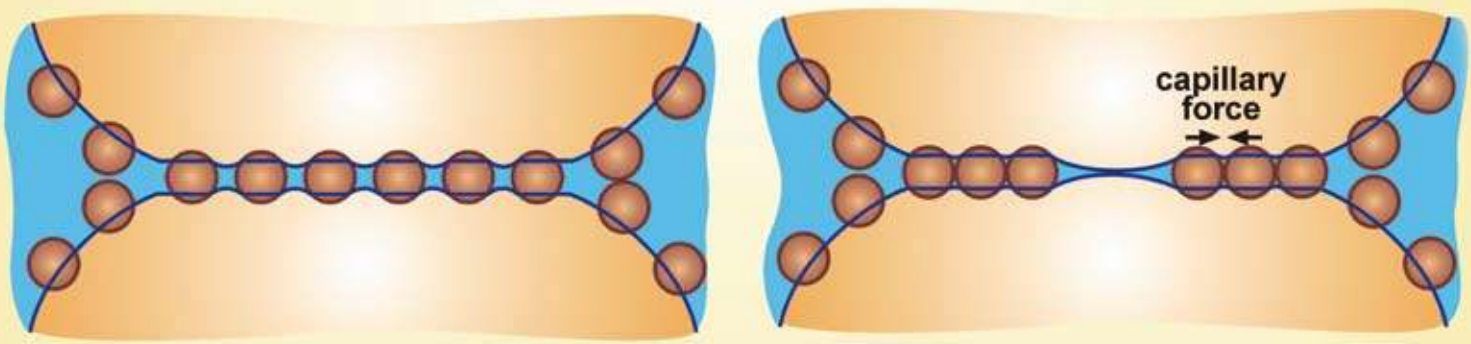

CAPILLARY FORCES

ISSN 1463-9076

1463-9076(2008)10:12;1-5

Comparison of solid particles, globular proteins and surfactants as emulsifiers†‡

S. Tcholakova,[a] N. D. Denkov*[a] and A. Lips[b]

Received 15th October 2007, Accepted 4th January 2008
First published as an Advance Article on the web 4th February 2008
DOI: 10.1039/b715933c

The aim of this paper is to present a short overview of the main mechanisms operative in the formation and stabilization of emulsions by solid particles and, on this basis, to make comparisons between solid particles, surfactants and globular proteins as emulsifiers. When available, simple quantitative relations are presented, with the respective numerical estimates and discussion of the applicability of these relations to particle-stabilized systems. Non-obvious similarities between the different types of emulsifiers are outlined in several cases in which the description of the system can be performed at a phenomenological level. Examples are presented for the process of emulsification, where we show that several simple theoretical expressions, derived originally in the studies of surfactants and protein emulsifiers, can be successfully applied to particle-stabilized emulsions. In contrast, for the phenomena in which the detailed mechanisms of particle adsorption and film stabilization are important, the differences between the various emulsifiers prevail, thus making it impossible to use the same theoretical description. The most important specific characteristics of the solid particles which strongly affect their behavior are the high barrier to particle adsorption, high desorption energy and strong capillary forces between particles trapped in liquid films, which all originate in the relatively large particle size (as compared to the size of surfactant and protein molecules). The capillary mechanism of stabilization of liquid films by solid particles is reviewed in some detail, to emphasize its specific features and to demonstrate the applicability of several simple expressions for approximate estimates. Interestingly, we found that the hypothesis for some exceptionally high coalescence stability of the particle-stabilized emulsions is not supported by the experimental data available in literature. On the other hand, the particles are able to completely arrest the process of Ostwald ripening in foams and emulsions, and this effect can be easily explained with the high desorption energy of the particles and the resulting capillary effects.

1. Introduction

Particle-stabilized emulsions and foams have attracted considerable research interest due to their unique properties and potential technological applications.[1–4] Some of the most interesting properties of these systems are related to the possibilities for (1) complete blocking of the process of Ostwald ripening, which is one of the main processes leading to bubble/drop coarsening in emulsions and foams;[5–7] (2) long-term stabilization either with a minimal amount of surfactant or without any surfactant; and [1–3] (3) fabrication of new materials with complex hierarchical structure by using particle-stabilized drops and bubbles as precursors.[4,8–12] In addition, the particle-stabilized emulsions and foams show some peculiar rheological properties, due to the irreversible particle adsorption and to the bridging of the surfaces of the neighboring droplets/bubbles by particle monolayers.[13–15] All these properties could be important for the current and some new applications of particle-stabilized emulsions and foams in food, pharmaceutical and personal care products, as well as for developing new structured materials.

These emulsions and foams have attracted growing interest from a scientific viewpoint, due to the fact that many of their properties cannot be explained with the common concepts developed in the studies of surfactant-stabilized systems. The first obvious differences are the bigger size of the particles and the fact that the solid particles, typically used for emulsion and foam stabilization, are non-amphiphilic (in contrast to the classical surfactants). Therefore, new theoretical models for a description of the particle attachment to the interfaces and for the particle stabilization of the foam and emulsion films were needed and have been developed during the years.[16–22] These models emphasized the important role of several specific features of the particle-stabilized dispersions which have no direct analogs in surfactant systems, such as the particle three-phase contact angle (as a measure of the particle

[a] *Laboratory of Chemical Physics & Engineering, Faculty of Chemistry, Sofia University, 1 J. Bourchier Ave., 1164 Sofia, Bulgaria. E-mail: nd@lcpe.uni-sofia.bg; Fax: +359 (0)2 962 5643; Tel: +359 (0)2 962 5310*
[b] *Unilever Global Research Center, Trumbull, Connecticut, 06611, USA*

† This article was submitted as part of a Theme Issue on colloidal particles at liquid interfaces. Other papers on this topic can be found in issue 48 of vol. 9 (2007). This issue can be found from the *PCCP* homepage [http://www.rsc.org/Publishing/Journals/CP/index.asp].
‡ The HTML version of this article has been enhanced with colour images.

hydrophobicity) and the strong interparticle capillary forces, as well as the irreversible character of the particle adsorption on the interfaces.[1–3,23,24]

The roles of these and many other factors were studied experimentally during the years.[1–3,23–28] In a series of recent papers, Binks and co-workers clarified experimentally the effect of a large number of factors on the type and stability of the formed emulsions, including the wettability, size and concentration of the solid particles; type of oil; pH; and electrolyte concentration.[1–3,29–33] Based on this deeper knowledge, more sophisticated particle-stabilized emulsions were developed.[32–35] In several impressive experimental studies,[11,23,24,36–39] the particle arrangement on single oil–water interfaces and in emulsion films was studied, and several non-trivial observations and conclusions were made. These studies revealed the presence of a strong, long-ranged (and unexpected) electrostatic repulsion between the particles adsorbed at the oil–water interface, as well as a very strong effect of the lateral capillary forces, especially between particles trapped in liquid films. The most important results from these studies are summarized in several recent reviews[1–4,7,28,37] and will not be reproduced here.

In parallel with the systematic experiments, several groups have developed theoretical models for description of the formation and stability of particle-stabilized emulsions. In a series of papers, Levine and Bowen[16–18] derived expressions for the free energy of formation of water-in-oil and oil-in-water emulsions, accounting for the formation of close-packed particle monolayers on the drop surface. More recently, Aveyard *et al.*[2,22] advanced this model by accounting for the effect of the line tension at the three-phase contact line. Aveyard *et al.*[2,22] also explored the effect of the curvature of the particle monolayers on the emulsion type and stability. The effect of the bending moment of the particle monolayers on the energy for emulsion formation was further elaborated by Kralchevsky *et al.*,[40] who proposed a thermodynamic criterion for the type of the formed emulsion (oil-in-water or water-in-oil). The detailed mechanism of stabilization of the emulsion films by solid particles was studied theoretically by Denkov *et al.*[19] and by Kruglyakov and Nushtayeva[20] who showed that the capillary forces play a decisive role in these systems (see section 3.1.3 below).

The experimental and theoretical results accumulated in recent years allowed the researchers to clarify the key elements in the mechanisms of formation and stabilization of particle-stabilized emulsions. However, the quantitative description of these systems is far from satisfactory and most of the theoretical models still lack experimental verification. Therefore, more systematic efforts for designing appropriate theoretical models, which are indeed able to describe quantitatively some of the characteristics of particle-stabilized emulsions, seem justified. One possible approach in this direction is to survey carefully the possibility for using/adapting some of the models, which were developed and verified during the years of research on emulsions stabilized by more "classical" emulsifiers (surfactants and proteins), for a description of the particle-stabilized emulsions. Obviously, such an approach should involve a clear distinction between the cases in which the "classical" approaches are applicable, from the cases in which the unique properties of the solid particles require a conceptually different description. Qualitative comparisons of the solid particles with the surfactants were made occasionally in the past,[1] but a systematic quantitative comparison has not been presented so far.

During the last several years, we had a chance to study emulsions stabilized by different types of emulsifiers, including low-molecular-mass surfactants, polymers, proteins and solid particles.[41–52] Both the emulsification[48–52] (mainly in turbulent flow) and the emulsion stability[41–47] were studied with quantitative experiments. In these studies, we observed some interesting similarities and differences between the various types of emulsifiers. One of the interesting observations was that the globular proteins behave either similarly to solid particles or to low-molecular-mass surfactants, depending on the specific experimental conditions (pH, electrolyte concentration *etc.*).[46,47] Thus in the course of these studies we were able to make various links between the different types of emulsifiers and to test several theoretical approaches with systematic experiments.

The major aim of this review is, based on our experience and on the results by other researchers, to make a short overview of the main mechanisms operative in the formation and stabilization of emulsions by solid particles, and to make comparison with the other types of emulsifiers. When available, simple quantitative relations are presented with the respective numerical estimates and the applicability of these relations to particle-containing systems is briefly discussed. By comparing the various emulsifiers, we were able to formulate some non-obvious conclusions (supported by experimental results or theoretical estimates) which are outlined throughout the paper.

The paper is structured as follows: in section 2 we compare the solid particles with the other types of emulsifiers (proteins and low-molecular-mass surfactants) with respect to their ability to facilitate drop breakage and to prevent drop–drop coalescence during emulsification. The similarities and the differences between the various emulsifiers are discussed and appropriate theoretical expressions for estimates of the various effects are presented. In section 3.1 the coalescence stability of emulsions containing various types of emulsifiers is compared and the mechanism of emulsion stabilization by solid particles is discussed. The mechanism for preventing Ostwald ripening by particle adsorption layers is briefly considered in section 3.2. The conclusions are summarized in section 4.

2. Emulsification—drop breakage and drop–drop coalescence

In this section we compare the solid particles to low-molecular-mass (LMM) surfactants and globular proteins, with respect to their action during emulsification in turbulent flow. The results presented and the related discussion are focused on the mean size of the drops formed during emulsification because this is the main characteristic of interest in the emulsification studies.

2.1 Regimes of emulsification in turbulent flow

The evolution of the mean drop size during emulsification is governed by the competition of two opposite processes—drop

breakage and drop–drop coalescence, see Fig. 1A. The relative contributions of these two processes on the final drop size distribution depend significantly on the type and concentration of the emulsifier used, the volume fraction of the dispersed phase and the hydrodynamic conditions.[48–50,53–55]

Several experimental studies showed[31,45,48,49,56] that for all types of emulsifiers (particles, surfactants and proteins) two qualitatively different regimes of emulsification are distinguished depending on the emulsifier concentration, see Fig. 1B. At low emulsifier concentration (in the so-called "emulsifier-poor" regime), the mean drop size rapidly decreases with the increase of emulsifier concentration, which is related to the important contribution of the drop–drop coalescence under these conditions. In contrast, at higher emulsifier concentrations the mean drop size is practically independent of the emulsifier concentration (emulsifier-rich regime) and is determined mostly by the process of drop breakup. Examples for these two regimes with emulsions stabilized by globular proteins and solid particles are presented in Fig. 1B.[45,48] Similar results were reported by other authors as well.[31,56]

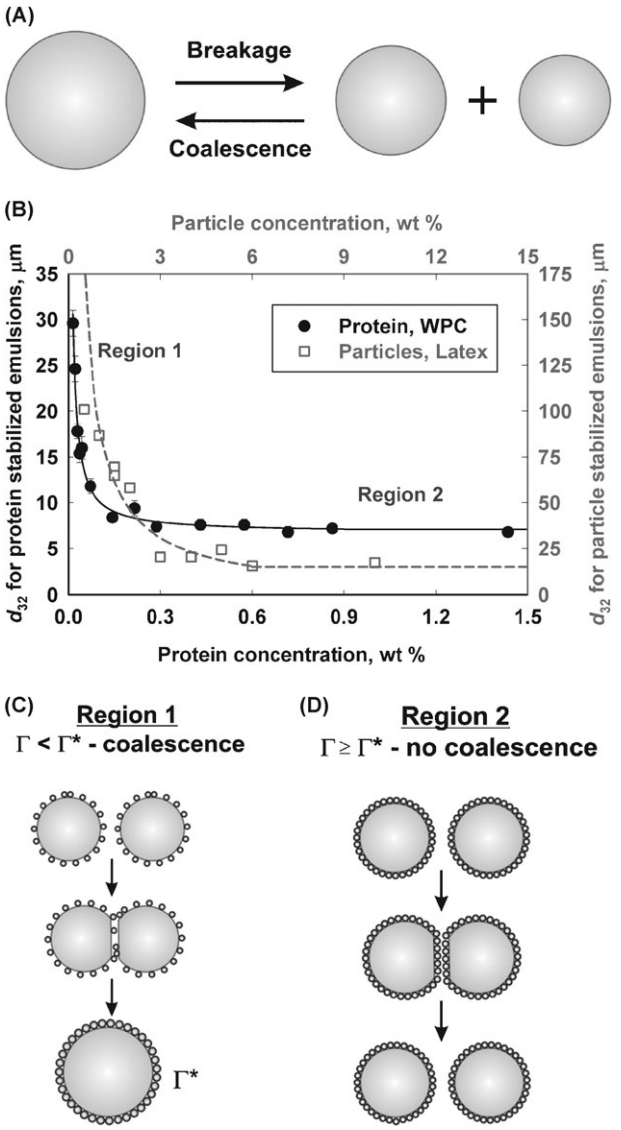

Fig. 1 (A) Schematic presentation of the two basic processes, governing the mean drop size during emulsification. (B) Mean volume–surface diameter, d_{32}, as a function of the initial emulsifier concentration for soybean oil-in-water emulsions stabilized by globular proteins (whey protein concentrate, full circles) and for water-in-hexadecane emulsions stabilized by latex particles (empty squares). In Region 1, the mean drop diameter, d_{32}, is affected strongly by drop–drop coalescence during emulsification, whereas d_{32} in Region 2 is determined exclusively by the process of drop breakage. Similar trends were reported for emulsions stabilized by ionic and nonionic surfactants.[49]

More detailed studies showed[46,49] that two different subregimes could be distinguished in the emulsifier-poor regime of emulsification. If the electrostatic repulsion between the emulsion droplets is suppressed (due to low electrical potential on the drop surface and high electrolyte concentration in the dispersed phase), the effect of drop–drop coalescence on the mean drop size can be described by a very simple phenomenological model, presented in section 2.2 below. In contrast, if the electrostatic repulsion between the drop surfaces is significant more complex models, which consider explicitly the surface forces acting between the colliding drops, are required to account for the drop–drop coalescence. Such a model, based on the Derjaguin–Landau–Verwey–Overbeek (DLVO) theory, was developed and verified with experimental data in ref. 49.

In the following two sections we present results for the cases of emulsifier-rich regime and emulsifier-poor regime with suppressed electrostatic repulsion, which can be described by simple theoretical models for all types of emulsifiers. The third sub-regime (surfactant-poor regime with significant electrostatic repulsion, realized at high surface potential and/or low electrolyte concentration) will not be considered here, because it is more system-specific.[49] Furthermore, no experimental results with particle-stabilized emulsions, which could allow us to test quantitatively the relevant theoretical models for this regime, are available. Note that a significant electrostatic barrier could appear between the solid particles and the drop surface in this regime, thus impeding particle adsorption—this effect is discussed in section 2.4.2 below.

2.2 Emulsifier-poor regime with suppressed electrostatic repulsions

This regime of emulsification is often realized when solid particles, nonionic surfactants or protein molecules are applied as emulsifiers in the presence of electrolytes with high concentration.[45,48,49] The comparison of the results obtained with various systems showed that when the electrostatic repulsion is suppressed there is a very close similarity between the action of the various emulsifiers. This similarity originates from virtually the same mode of drop stabilization during emulsification in this regime—an almost complete adsorption layer of particles/surfactant/protein must be formed on the drop surface to stop the drop–drop coalescence in these systems, see Fig. 1C. In other words, the initially formed drops (which are not covered with complete emulsifier layers) coalesce with each other until their surfaces become completely covered and protected by a dense layer of particles/

molecules.[45,48,49,57,58] The term ''partial coalescence'' was introduced to describe this mode of drop–drop coalescence.[57,58]

This mechanism of drop stabilization allowed several groups to propose a simple mass-balance model for prediction of the mean drop size after emulsification.[48,57] Various versions of this model were successfully applied to nonionic low-molecular-mass surfactants,[49] proteins[48,49] and solid particles.[45,57,58] The main idea of the model is that the drops coalesce during emulsification until the emulsifier adsorption on the drop surface reaches a certain threshold value, Γ^*, which is independent of the oil volume fraction and intensity of stirring. In the simplest version of this model an additional assumption is made, namely that most of the emulsifier in the system adsorbs on the drops surface, so that the amount of the non-adsorbed emulsifier is negligible in comparison with the total amount of emulsifier used. Under these assumptions, the following mass-balance which relates the initial emulsifier concentration and the mean volume-surface diameter of the drops, d_{32}, is derived for emulsions in which the emulsifier is initially dissolved/dispersed in the continuous phase:[48]

$$d_{32} \approx \frac{6\Phi}{(1-\Phi)}\frac{\Gamma^*}{C_{\mathrm{INI}}} = \frac{6\Phi}{(1-\Phi)}\frac{\theta^*\Gamma_{\mathrm{M}}}{C_{I\mathrm{NI}}} \qquad (1)$$

$$C_{\mathrm{SER}} = C_{\mathrm{INI}}\,(\text{emulsifier in the continuous phase})$$

Here C_{INI} is the initial emulsifier concentration in the continuous phase, C_{SER} is the concentration of the emulsifier left in the aqueous phase after emulsification, Φ is the volume fraction of the dispersed phase, Γ^* is the threshold adsorption required to stabilize the drops during emulsification, Γ_{M} is the emulsifier adsorption in a complete monolayer (*e.g.* a close-packed monolayer of solid particles), and $\theta^* = \Gamma^*/\Gamma_{\mathrm{M}}$ is the dimensionless threshold surface coverage.

Eqn (1) predicts that in the surfactant-poor regime the mean drop diameter d_{32} should be proportional to the inverse surfactant concentration, $1/C_{\mathrm{INI}}$. Also a strong dependence of d_{32} on the volume fraction of the dispersed phase, Φ, is expected, because more surfactant is needed to cover the larger amount of drops formed at higher Φ—at fixed d_{32} the drop surface area is proportional to Φ, whereas the amount of available surfactant is proportional to $(1-\Phi)$.

When the emulsifier is dissolved/dispersed in the droplets, the same approach leads to the following mass-balance, relating the initial emulsifier concentration to the mean drop diameter:[45]

$$d_{32} \approx \frac{6\Gamma^*}{C_{\mathrm{INI}}} = \frac{6\theta^*\Gamma_{\mathrm{M}}}{C_{\mathrm{INI}}} \qquad (2)$$

$$C_{\mathrm{SER}} = C_{\mathrm{INI}}\,(\text{emulsifier in dispersed phase})$$

Note that in this case d_{32} does not depend on the volume fraction of the dispersed phase, Φ, because both the drop surface area and the amount of available emulsifier are proportional to Φ at fixed d_{32} (so that the effect of Φ cancels out).

When particle-stabilized emulsions are considered, it is often more convenient to express the above equations in terms of the mean particle radius, a, and the initial weight concentration of the particles, C_{P} [in g L^{-1} or kg m^{-3}] (this concentration is defined with respect to the fluid phase, in which the particles are initially dispersed). Thus one obtains the following analogs of eqn (1) and (2):[45]

$$d_{32} \approx \frac{8\Phi}{1-\Phi}\frac{\pi a^3\rho_P}{C_P}\Gamma^* = \frac{8\Phi}{1-\Phi}\frac{a\rho_P\phi_{CP}}{C_P}\theta^*(\text{particles in the continuous phase}) \qquad (3)$$

$$d_{32} \approx \frac{8a\rho_{\mathrm{p}}\varphi_{\mathrm{CP}}}{C_{\mathrm{p}}}\theta^*(\text{particles in the dispersed phase}) \qquad (4)$$

where φ_{CP} is the fraction of the surface area that is covered by adsorbed particles in a complete monolayer (for spherical particles $\varphi_{\mathrm{CP}} = \pi/(12)^{1/2} \approx 0.907$) and ρ_{p} is the particle mass density.

The predictions of the above equations were confirmed in several independent studies with all basic types of emulsifiers,[45,48,49] see Fig. 2. The fits of the experimental data for the dependence of d_{32} on $1/C_{\mathrm{INI}}$ showed that in most cases $\theta^* \approx 1$, for all types of emulsifiers. In other words, in this regime of emulsification (low emulsifier concentration, suppressed electrostatic repulsion) a complete adsorption monolayer should be usually formed for preventing the further drop–drop coalescence during emulsification. In some of the studies with solid particles, $\theta^* \approx 3$ was measured and explained[45] with the strong aggregation of the particles in the systems studied—this aggregation leads to formation of particle adsorption multilayers on the drop surface, so that a larger number of particles is needed to completely cover this surface.

It is worth noting that the emulsions obtained in this regime remain stable for a long time upon shelf-storage which is not always the case with the emulsions obtained in the other regimes of emulsification (see ref. 49). This result indicates that the detailed mechanisms of drop stabilization during emulsification in this regime should be similar to the mechanisms which ensure the long-term stability of the respective emulsions.

We thus conclude that in this regime of emulsification: (1) a complete adsorption layer of emulsifier should be formed on the drop surface for preventing the drop–drop coalescence and (2) the mean drop size in these systems can be estimated by eqn (1)–(4). Note that in this sub-section we have not specified the hydrodynamic conditions of emulsification (turbulent or regular flow). Therefore, the models discussed above are applicable to any type of hydrodynamic conditions, provided that the other assumptions of the model are satisfied.

Let us mention at the end that the above consideration is applicable only to the case of negligible barriers to particle adsorption on the oil–water interface. If the adsorption barrier is significant, *e.g.* because of strong electrostatic repulsion between the solid particles and the drop surface, the particle adsorption could be hindered and the above mass balances become inapplicable (see section 2.4.2 below).

2.3 Emulsifier-rich regime of emulsification in turbulent flow

In this regime of emulsification, the mean drop size does not depend on emulsifier concentration (see Fig. 1B). This means that the drop–drop coalescence is suppressed by the adsorbed species and hence the drop size is determined exclusively by the

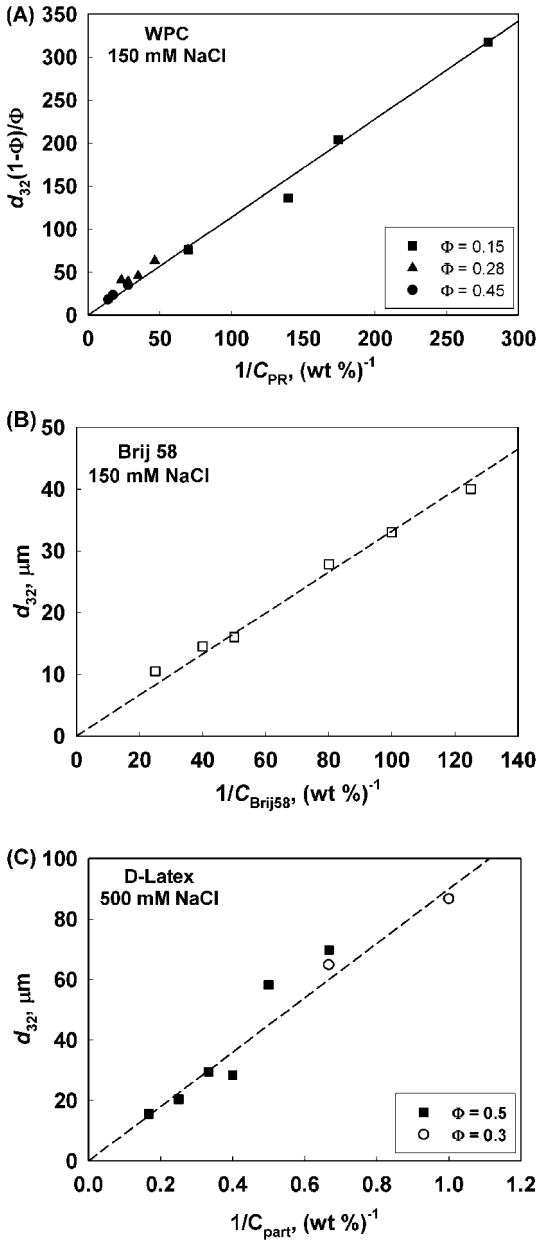

Fig. 2 Mean diameter, d_{32}, as a function of the inverse initial emulsifier concentration for emulsions stabilized by (A) protein concentrate WPC,[48] (B) nonionic surfactant Brij 58,[49]49 and (C) latex particles.[45]

process of drop breakup.[49,50,52] The emulsifier concentration at which the transition between the emulsifier-poor and the emulsifier-rich regimes occurs depends significantly on the type of emulsifier, electrolyte concentration, type and size of used particles, volume fraction of the dispersed phase, hydrodynamic conditions and several other factors, which are discussed in ref. 45, 46, 48 and 49 and will not be considered here. In the following consideration we discuss the emulsification in turbulent flow, because most of the quantitative results are obtained in this regime.

The first successful theory for description of the drop breakup process in turbulent flow was developed by Kolmogorov[59] and Hinze.[60] According to their theory, the maximal diameter, d_K, of the drops that are not broken inside the turbulent flow (the so-called "maximal stable drops") is estimated by comparing the drop capillary pressure, $P_C = 4\sigma/d$ (σ is interfacial tension), with the average magnitude of the fluctuations in the hydrodynamic pressure of the fluid, $\langle \Delta P_T(d) \rangle \approx \rho_C \langle u \rangle^2 \approx \rho_C (\varepsilon d)^{2/3}$, which in turn is expressed through the average rate of energy dissipation per unit mass of the emulsion, ε [J kg^{-1} s^{-1}] and the mass density of the continuous phase, ρ_C (for detailed explanations see ref. 59 and 60). From the comparison, $P_C \approx \langle \Delta P_T(d) \rangle$, the following expression for d_K was derived theoretically[59,60] and confirmed experimentally[61] for emulsions prepared with pure oil and water phases (without using any emulsifier):

$$d_K = A_1 \varepsilon^{-2/5} \sigma^{3/5} \rho_C^{-3/5} = A_1 d_{KI} \text{ (negligible drop viscosity)} \quad (5)$$

where A_1 is a numerical constant of the order of unity and the combination $d_{KI} \equiv \varepsilon^{-2/5} \sigma^{3/5} \rho_C^{-3/5}$ has the dimension of length.

The Kolmogorov–Hinze model was originally developed for breaking drops with relatively low viscosity.[59,60] The model was further upgraded by Davies[62] and by Calabrese *et al.*[63–65] for viscous drops, by including the viscous stress inside the breaking drops in the total stress balance describing the breakage process. The following expression for the maximum stable diameter of drops with viscosity η_D was derived:[62]

$$d_D = A_1 \left(1 + A_2 \frac{\eta_D \varepsilon^{1/3} d^{1/3}}{\sigma} \right)^{3/5} d_{KI} \text{ (significant drop viscosity)} \quad (6)$$

where A_2 is another numerical constant. The second term in the right-hand side of eqn (6) expresses the relative contribution of the energy of viscous dissipation in the breaking drop, normalized by the drop surface energy. At low viscosity of the dispersed phase, η_D, the viscous contribution becomes negligible and eqn (6) reduces to eqn (5). On the basis of theoretical considerations or experimental data, various values of the constants A_1 and A_2 were proposed in the literature.[50,61–65] For discussion of the possible origin of the discrepancy between these values, see ref. 50. Recently, $A_1 \approx 0.86$ and $A_2 \approx 0.37$ were determined in experiments at well-defined hydrodynamic conditions,[50] which are in good agreement with theoretical estimates,[62] and these values will be used below for comparison with the experimental data.

As seen from eqn (5) and (6), in the emulsifier-rich regime of emulsification, the emulsifier affects the drop breakage mainly through the value of the interfacial tension. To compare the theoretical predictions with experimental results obtained with different types of emulsifiers, we plot in Fig. 3 data for tetradecane-in-water emulsions, stabilized by LMM surfactants and proteins, and for water-in-tetradecane emulsions stabilized by latex particles. All these results are obtained by emulsification in turbulent flow, at sufficiently high emulsifier concentrations to be in the emulsifier-rich regime. The comparison of eqn (5) with the experimental data shows a reasonable agreement for all systems studied. One particular feature of the solid particles and the proteins in this context was that we should use the dynamic interfacial tension of the respective systems to describe the experimental data (while the

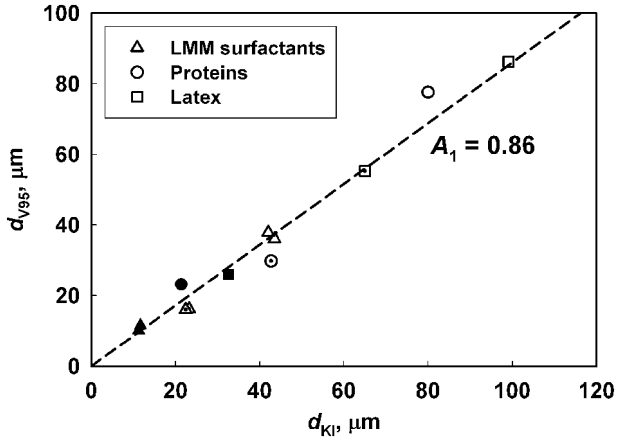

Fig. 3 Correlation plot for the theoretically predicted values of the maximum drop diameter, dKI, (see eqn (5)) and the corresponding experimental values, d_{V95}d for tetradecane-in-water emulsions stabilized by LMM surfactants (triangles), proteins (circles) and water-in-tetradecane emulsion stabilized by latex particles (empty squares), prepared with an Ultra Turrax rotor-stator homogenizer (operating in turbulent regime of emulsification) at different rotation speeds.

equilibrium interfacial tension was used for LMM surfactants), which is due to the much slower kinetics of particle/protein adsorption, as compared to the adsorption of LMM surfactant molecules.[50] In fact, for the particle-stabilized systems, the interfacial tension of the bare oil–water interface should be used in eqn (5) and (6) because the surface pressure of the particle adsorption layers is almost zero until the particles cover the interface with a complete, close-packed monolayer.[66]

Summarizing this section, the mean drop size in the emulsifier-rich regime of emulsification depends on the used emulsifier exclusively through the interfacial tension, see eqn (5) and (6). The main difference of the particles and proteins on one side from the LMM surfactants on the other side, is the much faster adsorption kinetics of surfactants. A direct consequence of this difference is the necessity of using in eqn (5) and (6) the dynamic surface tension for proteins and the interfacial tension of the bare oil–water interface for the particles, whereas the equilibrium surface tension can usually be used for LMM surfactants. For additional experimental results and more detailed discussion on this point see ref. 50.

2.4 Main differences between the various types of emulsifiers with respect to emulsification

As shown in the previous two sections, the mean drop size after emulsification could be described in many cases by the same equations, irrespective of whether particle-, surfactant- or protein-stabilized emulsions are considered. However, there are many other cases in which the particles as emulsifiers behave differently from proteins and surfactants. These differences are due mostly to the following three features of the solid particles: slower kinetics of adsorption due to the larger amount of material needed to cover drop surfaces, high barrier to particle adsorption and very high desorption energy. All these features are related to the relatively large size of the particles (typically between 10 nm and 5 μm), as compared to the typical surfactant molecules (between 0.4 and 1 nm) and protein molecules (between 1 and 5 nm).

The effects of the slow kinetics and of the high barrier to particle adsorption can strongly affect the emulsification process and are discussed in the following sections 2.4.1 and 2.4.2. The high desorption energy of the particles mostly affects the mechanisms of emulsion stabilization against drop–drop coalescence and Ostwald ripening—these effects are considered in sections 3.1 and 3.2 respectively.

2.4.1 Characteristic times for barrier-less adsorption of the various emulsifiers. First, we compare the characteristic time for barrier-less emulsifier adsorption, t_A, on one side with the characteristic times of drop deformation, t_D, and of drop–drop contact, t_C, in the flow. If t_A is shorter than t_D and t_C, the drop breakup and the drop–drop contact occur with drops whose surfaces are covered with (almost) equilibrium adsorption layers. In contrast, when the adsorption is slow the drop breakup and collisions occur with drops whose surfaces are covered with lower than equilibrium adsorption layers, see Fig. 4.

Expressions for estimating the various characteristic times for both turbulent and shear flows can be found in the literature:[49,53,67,68]

(a) Drop deformation times, t_D for viscous drops ($\eta_D \gg \eta_C$) can be estimated from the expressions:[49,67,68]

$$t_D \approx \frac{\eta_D}{\rho_C \varepsilon^{2/3}} \frac{1}{d^{2/3}} \quad \text{(viscous drop, inertial turbulent flow)} \tag{7}$$

$$t_D \approx \frac{\eta_D}{\eta_C} \frac{1}{\dot{\gamma}} \quad \text{(viscous drop, laminar flow)} \tag{8}$$

where η_D and η_C are the dynamic viscosities of the drop phase and of the continuous phase respectively, ρ_C is the mass density of the continuous phase, ε is the rate of energy dissipation per unit mass of the fluid in the turbulent flow, $\dot{\gamma}$ is the shear rate of the regular flow, and d is the drop diameter.

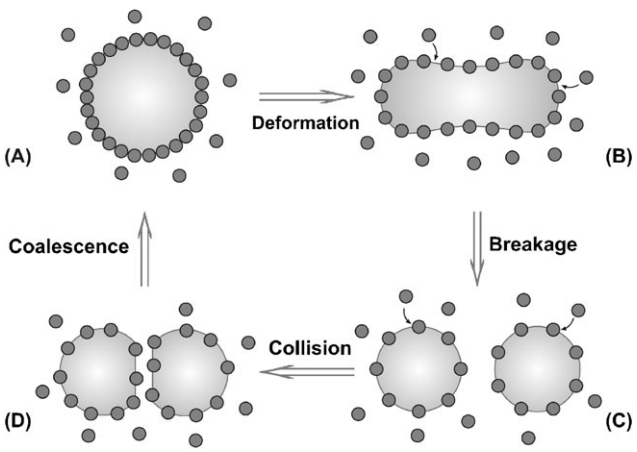

Fig. 4 Schematic presentation of the process of drop deformation (A) to (B); drop breakage (B) to (C); collision (C) to (D) and coalescence (D) to (A), if the emulsifier adsorption time, t_A, is longer than the drop deformation time, t_D, and the collision time, t_C.

Drop deformation times, t_D, for low-viscosity drops ($\eta_D \sim \eta_C$) can be estimated from the expressions:[54,68,69]

$$t_D \approx \frac{d^{2/3}}{\varepsilon^{1/3}} \quad \text{(low-viscosity drop, inertial turbulent flow)} \tag{9}$$

$$t_D \approx \frac{1}{\dot{\gamma}} \quad \text{(low-viscosity drop, laminar flow)} \tag{10}$$

To estimate the characteristic time of drop deformation in viscous turbulent flow, one can use the expressions for laminar flow eqn (8) and (10), taking into account that $\dot{\gamma} \approx (\varepsilon\rho_C/\eta_C)^{1/2}$ for this flow, for details see ref. 49 and 70.

(b) Characteristic times of drop–drop contact, t_C, can be estimated by the expressions:[49,54,67,70]

$$t_C \approx \frac{d^{2/3}}{\varepsilon^{1/3}} \quad \text{(inertial turbulent flow)} \tag{11}$$

$$t_C \approx \frac{1}{\dot{\gamma}} \quad \text{(laminar flow)} \tag{12}$$

(c) Characteristic adsorption times, t_A, can be estimated by the expression:[49,67,68]

$$t_A \approx \frac{\Gamma_M}{j} \tag{13}$$

where Γ_M is the emulsifier adsorption on the drop surface at dense adsorption monolayer and j is the flux of surfactant toward the drop surface (per unit area). Depending on the predominant mechanism of surfactant transport to the drop surface (convective or diffusive) the emulsifier flux is given by different expressions. In turbulent flow and at high shear rates the convective term is usually predominant, which corresponds to high Peclet numbers, $Pe = Ud/D \gg 1$, where U is the characteristic velocity of the flow and D is the diffusion coefficient of the emulsifier entities. In this case, the flux to the surface can be estimated as $j \sim CU$, where C is the emulsifier concentration in the continuous phase.

In such a convection-dominated adsorption regime, the following equations for the characteristic adsorption times are used, depending on the flow type:[67]

$$t_A \approx \frac{\Gamma_M}{C(\varepsilon d)^{1/3}} \quad \text{(inertial turbulent flow)} \tag{14}$$

$$t_A \approx \frac{\Gamma_M}{Cd\dot{\gamma}} \quad \text{(laminar flow)} \tag{15}$$

From the above expressions one sees that the contact time, t_C, and the drop deformation time, t_D, depend on the drop size, the flow characteristics and the viscosity of the dispersed phase, η_D. Therefore, these times do not depend directly on the emulsifier used. The specific effects of the emulsifier are reflected only in the adsorption time, t_A, which in turn determines the instantaneous emulsifier adsorption, $\Gamma(t)$, during the processes of drop deformation and collision. For this reason, the following discussion is focused on the comparison of the characteristic adsorption times, t_A, of the different emulsifiers.

From eqn (14) and (15) we see that the emulsifier appears in the estimates of t_A through the ratio of the emulsifier adsorption in the complete monolayer, Γ_M, and the bulk emulsifier concentration, C. Numerous experimental studies showed that the typical values of Γ_M are of the order of 1.5–2 mg m^{-2} for both the LMM surfactants and proteins.[49,71–73] Therefore, both the ratio Γ_M/C and the characteristic adsorption times t_A are similar for surfactants and proteins at equal bulk concentration C. In other words, no significant difference is expected for the rate of *barrier-less* adsorption of surfactants and proteins.

In contrast, the mass of the adsorbed material per unit area for a complete monolayer of adsorbed spherical particles, $\Gamma_M \approx \rho_P\varphi_{CP}(4\pi a^3/3)/(\pi a^2) \approx 4\rho_P\varphi_{CP}a/3$, is proportional to the particle radius, whereas the bulk mass concentration of particles is independent of a (the relations for non-spherical particles are similar, as well). Therefore, in particle-stabilized emulsions, the ratio Γ_M/C and the adsorption time, t_A, increase linearly with the particle size. In other words, the bigger particles will adsorb more slowly in comparison with the small nanoparticles, proteins and surfactant molecules (at equal bulk concentration by weight, C), mainly due to the larger demand of material that should be adsorbed to cover completely the drop surfaces. This is one of the main reasons for the experimental observations that higher weight concentrations of particles are needed when particle-stabilized emulsions are prepared (typically a few percent), whereas concentrations as low as 0.01 to 0.1 wt% are sufficient to make stable emulsions with micrometer-sized drops when using proteins and LMM surfactants.[45,48,49,56] The other significant reason, namely the adsorption barrier which is much more pronounced for the solid particles (as compared to surfactants and proteins), is considered in the following section.

2.4.2 Role of the electrostatic barrier to particle adsorption. If charged particles are dispersed in polar phase at low electrolyte concentrations, significant electrostatic repulsion may appear[49] when the particles approach the oil–water interface, which is usually charged.[74] This repulsion may strongly hinder particle adsorption so that the equations for the mean drop size in sections 2.2 and 2.3 and the estimates of t_A in section 2.4.1 become inapplicable. The main effect of the adsorption barrier is to significantly reduce the probability of particle attachment to the interface, so that the particle adsorption layers remain incomplete. As a result, significant drop–drop coalescence and phase separation may occur during and after emulsification, even at high particle concentrations.[1,45]

To assess theoretically the importance of the adsorption barrier during emulsification, one can compare the maximal repulsive force, F_{MAX}, acting between the particle and drop surface, with the hydrodynamic force pushing the particle toward this surface. The interaction force between a spherical particle with radius, a, and spherical oil drop with radius, R, can be estimated by Derjaguin's formula:[75,76]

$$F(h) = \frac{2\pi aR}{R+a}\int_h^\infty \Pi(h)\mathrm{d}h \approx 2\pi a\int_h^\infty \Pi(h)\mathrm{d}h \quad \text{(particles immersed in polar phase)} \tag{16}$$

$$h << a << R$$

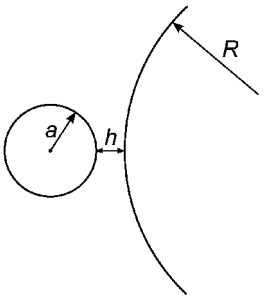

Fig. 5 Schematic presentation of the liquid gap formed between a small solid particle with radius, a, and a bigger drop with radius R.

where $\Pi(h)$ is the force per unit area (disjoining pressure) that would act between two planar surfaces, one of them being the oil drop surface and the other one having the same properties as the particle surface, and h is the distance between particle forehead and drop surface, Fig. 5. One sees from eqn (16) that for small particles ($a \ll R$) the interaction force, $F(h)$, is proportional to particle radius, a.

For fractal solid particles (*e.g.* fumed silica), one should use the radius of the primary particles as a characteristic size in eqn (16), composing the fractal structure.[77,78] For edged particles with regular (cubic, needle-like *etc.*) or irregular shapes, the radius of curvature of the particle edges has to be used in eqn (16) because it is easier for the sharp edges to overcome the barrier and to make a contact with the fluid surface.[77–79] Because the size of primary particles and the radius of curvature of the particle edges are typically very small ($\approx$10–50 nm), the adsorption barrier is much lower for fractal and edged particles, as compared to smooth-shaped particles (spheres, ellipsoids) with the same overall size.

To make use of eqn (16), we should specify the disjoining pressure in the film separating the surfaces of the solid particle and the drop, $\Pi(h)$. For the following estimates, we use the simplest possible expressions, combining van der Waals and electrostatic forces, $\Pi(h) = \Pi_{VDW}(h) + \Pi_{EL}(h)$.[75,76,80–82] The van der Waals component is given by the expression $\Pi_{VDW}(h) \approx A_H/6\pi h^3$, where A_H is the Hamaker constant. The electrostatic component can be estimated by one of the following expressions:[76,82]

$$\Pi_{EL}(h) \approx \frac{\varepsilon_r \varepsilon_{r0} \kappa^2}{2\pi} \frac{2\psi_{S1}\psi_{S2}\cosh \kappa h - (\psi_{S1}^2 + \psi_{S2}^2)}{\sinh^2 \kappa h} \quad \text{(low surface potentials, } \frac{e\psi_S}{k_B T} < 1) \tag{17}$$

$$\Pi_{EL}(h) \approx 64 n_0 k_B T \tanh\left(\frac{e\psi_{S1}}{4k_B T}\right) \tanh\left(\frac{e\psi_{S2}}{4k_B T}\right) \exp(-\kappa h) \quad \text{(weak overlap of the electric double layers, } \kappa h \gg 1) \tag{18}$$

where ε_r and ε_{r0} are relative and vacuum dielectric constants respectively; ψ_{S1} and ψ_{S2} are surface potentials of the drop and particle; n_0 is electrolyte concentration; k_B is the Boltzmann constant; T is temperature; e is elementary electric charge, and κ is the Debye screening parameter (all equations are given for 1 : 1 electrolyte). If the surface potentials of the particle and the drop are lower than *ca.* 25 mV, eqn (17) is more appropriate because it is valid at arbitrary film thickness, h. If either of the surface potentials is high eqn (18) is preferred, keeping in mind that it might overestimate the electrostatic barrier by several times, because the maximum in the force $F(h)$ usually appears at $\kappa h \approx 1$, whereas the weak-overlap approximation requires $\kappa h \gg 1$. For more accurate estimates, the rigorous non-explicit expressions derived by Derjaguin[75,76] could be used.

The repulsive barrier between the particle and the drop surface, F_{MAX}, is found as the maximum in the dependence $F(h)$. Due to the complex dependence of $F(h)$ on C_{EL} and h, F_{MAX} has to be found by numerical calculations. Expressions for other possible components of disjoining pressure (hydrophobic, steric, ion-correlation forces, hydration repulsion *etc.*), which can be used for numerical estimates of F_{MAX} are available in the literature.[80–82].

For turbulent flow, the hydrodynamic force pushing the particles toward the drop surface can be estimated by the expression:[83]

$$F_T \sim \left(\frac{aR}{a+R}\right)^2 \langle \Delta P_T \rangle \sim \left(\frac{aR}{a+R}\right)^2 \rho_C \langle u^2 \rangle \sim \left(\frac{aR}{a+R}\right)^2 \rho_C \varepsilon^{2/3} (a+R)^{2/3} \sim a^2 \rho_C \varepsilon^{2/3} R^{2/3} \text{(inertial turbulent flow)} \tag{19}$$

where $\langle u^2 \rangle$ here is the mean square of the fluctuations in the turbulent velocity at distances of the order of drop radius, R. Eqn (19) predicts that the hydrodynamic force depends on the intensity of stirring through the multiplier $\varepsilon^{2/3}$ and, for large drops with $R \gg a$, is proportional to a^2.

For simple shear flow, the hydrodynamic force pushing the particle toward the drop surface can be estimated as a product of the shear stress created by the fluid motion and the particle cross-section, πa^2. For approximate estimates one can assume that the rate of shear flow in close vicinity to the drop surface is of the same order of magnitude as the shear rate in the bulk medium, $\dot{\gamma}$ (the exact calculation of the flow profile and the resulting hydrodynamic force is a very difficult hydrodynamic problem):[84]

$$F_S r \sim \eta_C a^2 \dot{\gamma} \quad \text{(shear flow)} \tag{20}$$

Eqn (19) and (20) should be considered as very approximate estimates, because they do not account directly for the effect of the drop on the hydrodynamic flow around its surface.

Let us compare numerically the electrostatic barrier with the hydrodynamic forces, under typical conditions for emulsification in turbulent and shear flows. Taking a = 100 nm, R = 10 μm, $\rho_C = 10^3$ kg m^{-3} and $\varepsilon = 10^5$ J kg^{-1} s^{-1} (typical for a lab-scale rotor–stator or narrow-gap homogenizers),[47–49,61] one estimates $F_T \approx 10^{-11}$ N for turbulent flow. Taking $\dot{\gamma} = 10^2$ s^{-1}, typical for stirring by lab-scale mixer and for emulsion flow in a pipe,[85] one estimates $F_S \approx 10^{-15}$ N. The scaling of these forces with the particle and drop radii, and with the flow intensity, is clear from eqn (19) and (20).

The height of the electrostatic barrier, F_{MAX}, is very system-specific. Taking for estimate the values $\psi_{S1} \approx \psi_{S2} \approx -25$ mV, $A_H \approx 10^{-20}$ J, and C_{EL} = 1 mM, we calculate $F_{MAX} \approx 2 \times 10^{-12}$ N for a = 100 nm, which is to be compared with F_T and

F_S estimated in the preceding paragraph. Due to the different dependences on the particle radius, a, of the adsorption barrier on one side, and of the hydrodynamic forces on the other side, the bigger particles could be able to overcome the adsorption barrier, whereas the small particles might be unable to adsorb when all other conditions are the same. Note that F_{MAX} depends strongly on electrolyte concentration and the electrostatic barrier disappears at *ca.* $C_{EL} > 150$ mM.[42,46]

In the following we show that the above equations can be used to explain several important experimental results reported in the literature. In ref. 57, silica particles with $a =$ 25 nm were used to stabilize PDMS-in-water emulsions. The experiments showed that a significant excess of particles was needed for emulsification by hand-shaking, as compared to emulsification by jet-homogenizer. Taking $\psi_{S1} \approx -25$ mV for the silica surface,[86–88] $\psi_{S2} \approx -60$ mV for the PDMS–water interface,[86–88] and $C_{EL} = 10^{-4}$, we calculate $F_{MAX} \approx 5.7 \times 10^{-12}$ N, which is lower than the hydrodynamic forces in the jet homogenizer, $F_T \approx 1 \times 10^{-11}$ N ($R = 1$ μm, $\varepsilon \approx 10^8$ J kg^{-1} s^{-1} according to ref. 83), and higher than the force $F_T \approx 6 \times 10^{-13}$ N during emulsification by hand-shaking ($\varepsilon \approx 10^3$ J kg^{-1} s^{-1}). Therefore, the hydrodynamic force in the jet-homogenizer was sufficiently strong to push the particles over the electrostatic adsorption barrier, whereas the hydrodynamic force during hand-shaking was relatively weak, thus leading to reduced particle adsorption. In conclusion, either high particle concentration (at mild stirring) or intensive stirring (at lower particle concentration) is required for collecting a sufficient number of adsorbed particles on drop surface in the presence of adsorption barrier.

Similar estimates could explain the strong effect of electrolytes, reported in ref. 45 for water-in-oil emulsions, stabilized by latex particles with radius $a \approx 100$ nm. The estimated interaction force between particles with $\psi_{S1} \approx -80$ mV (measured by us) and tetradecane–water interface with $\psi_{S2} \approx -40$ mV,[49,74] at electrolyte concentration $C_{EL} = 10$ mM, is $F_{MAX} \approx 3 \times 10^{-10}$ N. This barrier is higher than the hydrodynamic force $F_T \approx 1 \times 10^{-11}$ N ($R = 10$ μm, $\varepsilon \approx 10^5$ J kg^{-1} s^{-1}). As a result, the particle adsorption is suppressed at low electrolyte concentrations, and the drops intensively coalesce with each other during and after emulsification, unless an excess of particles (several wt%) is used. In contrast, at high electrolyte concentrations, $C_{EL} = 500$ mM, the electrostatic barrier disappears and particle concentration of 1 wt% is sufficient to obtain stable emulsions.[45]

At the qualitative level, the electrostatic barrier could also explain the differences typically observed when latex and silica particles are applied as emulsifiers.[1–3,45,89] Latex particles are usually more charged and larger in size than the silica particles (the latter often being with fractal structure)—both factors lead to a much higher adsorption barrier for the latex particles. This comparison explains why it is easier to obtain emulsions stabilized by silica[1–3,29–32] and why the electrolyte concentration is crucial when latex particles with $a > 50$ nm are used for emulsion and foam stabilization.[1,45]

The electrostatic barrier could be efficiently suppressed by neutralizing the particle charge through the addition of oppositely charged surfactants or multivalent counterions, or by adjusting pH, and/or *via* screening of the electrostatic repulsion with electrolytes of high concentration.[1,29,45,90,91] However, the same factors suppress the electrostatic repulsion between the particles themselves and the particles tend to flocculate under these conditions. Thus one explains the experimental observation that stable emulsions are often obtained under conditions, corresponding to weakly flocculated particles.[1,45,91]

Note that a similar barrier appears when charged surfactant or protein molecules approach an oil–water or air–water interface.[21,92–94] One can estimate from the above equations that the hydrodynamic forces are rather weak compared to the electrostatic forces for such small molecules ($a \leq 2$ nm). For this reason, Brownian motion is more efficient as a transport mechanism for the adsorption of small surfactant and protein molecules, and for nanoparticles of similar size. The relevant adsorption barrier for Brownian transport is the maximal energy of repulsion, W_{MAX}, scaled with the thermal energy because a Boltzmann factor appears in the stochastic problem for overcoming an energy barrier by diffusion, $\exp(-W_{MAX}/k_BT)$.[95,96] For solid particles, W_{MAX} can be estimated from the interaction energy between the particle and the fluid surface, $f(h)$, by using another form of Derjaguin approximation:[75,76,80,82]

$$W(h) \approx 2\pi a \int_h^\infty f(h)\mathrm{d}h; f(h) = \int_h^\infty \Pi(h)\mathrm{d}h \qquad (21)$$

From the equations presented above one can estimate that the energy barrier is typically very high for solid particles, $W_{MAX}/k_BT \gg 1$, which evidences that Brownian motion is inefficient for overcoming the adsorption barrier by solid particles, except for small nanoparticles with $a < 2$ nm. In contrast, W_{MAX} is typically of the order of several k_BT units for surfactant and protein molecules.

Thus we can conclude that Brownian motion is the main transport mechanism for overcoming the adsorption barriers by surfactant and protein molecules, whereas the convective transport usually governs the attachment of bigger particles to oil–water interfaces. Some intermediate range exists for the size of spherical particles (*ca.* 2 nm $< a <$ 25 nm), in which neither of these mechanisms is very efficient in facilitating particle adsorption. Further quantitative studies are needed to clarify the domains in which one or another mechanism of particle transport dominates—for solving this problem, some of the approaches developed in the area of froth-flotation to describe particle–bubble interactions[97,98] could be useful.

2.4.3 Electrostatic interactions for particles dispersed in the non-polar phase. In a recent study, Danov *et al.*[99] considered theoretically the electrostatic interactions between particles pre-dispersed in a non-polar (oily) phase and the respective oil–water interface. By considering the interactions which appear when electrically charged particle approaches the fluid interface, they showed that a strong electrostatic attraction could appear, due to the so-called "image forces" between the charges distributed on the particle surface and the fluid interface. The following expression for the respective interaction

force between the particle and fluid interface was derived:[99]

$$F(h) \approx -\frac{Q^2}{\varepsilon_{2r}[2(a+h)]^2} \approx -4\pi^2\sigma_{EL}^2 a^2/\varepsilon_{2r} \quad (22)$$

(particles immersed in the non-polar phase)

where Q is the particle charge, ε_{2r} is the dielectric constant of the medium, in which the particle is dispersed, and $\sigma_{EL} = Q/4\pi a^2$ is the electric charge density on the particle surface. The numerical estimates in ref. 99 showed that, for typical values of the governing parameters (silica or glass particles immersed in tetradecane), the image–force interaction becomes significant for particles with radius $a > 30$ nm. Thus an attraction force appears when a charged particle is approaching the oil–water interface from the oil phase. The authors used this theoretical prediction to suggest that the water drops attract the charged hydrophobic particles predispersed in the oily phase, thus favoring the formation of inverse particle-stabilized emulsions. One should note, however, that the strong electrostatic repulsion between such charged particles should keep the adsorbed particles on the surface at a distance from each other,[38,39] thus preventing the formation of dense adsorption layers and reducing emulsion stability.

3. Long-term emulsion stability

In section 2 we clarified the regimes of emulsification and the related phenomena, in which the solid particles behave similarly to the LMM surfactants and proteins, and discussed the reasons why the particles behave differently in the other cases. Not surprisingly, we found that close similarities are observed in these cases, in which the effect of the emulsifier could be described by basic phenomenological relations and quantities only—see eqn (1)–(6) for examples. For the phenomena and processes in which the specific interactions and mechanisms are important (*e.g.* the adsorption barrier of molecules and particles), significant differences emerge, mainly due to the different size, energy and force scales for the various types of emulsifier entities.

When working on the current section, devoted to the long-term stability of emulsions, we also found that some similarities could be outlined when phenomenological thermodynamic and mechanical relations are used, *e.g.* when balances including disjoining, capillary, hydrostatic or two-dimensional surface pressures are made, without paying attention to the specific mechanism of stabilization (see *e.g.* eqn (23) and (24) below). In the other cases, the differences between the solid particles and surfactants are very profound, the main reason being the very specific capillary mechanism of emulsion stabilization by the particles.

Because the literature on emulsion stabilization by LMM surfactants is vast,[27,100–102] whereas the studies considering the capillary mechanism of stabilization by particles are very limited,[19,20,39] we decided to focus the presentation in the following two sections on the role of capillary forces in the particle-stabilized emulsions. In addition, we compare the experimental data on emulsion stability for the different types of emulsifiers, to check the widely-spread notion that the particle-stabilized emulsions are exceptionally stable.

The analysis of the respective data with proteins[46,47] showed that under some conditions the proteins behave similarly to surfactants, under other conditions to solid particles, and under a third set of conditions they exhibit specific features, mostly related to the ability of the adsorbed protein molecules to slowly rearrange and to form strong covalent and non-covalent intermolecular bonds.[43] These cases are distinguished below whenever appropriate.

3.1 Long-term emulsion stability with respect to drop–drop coalescence

3.1.1 Comparison of the emulsifiers with respect to emulsion coalescence stability. In this section we compare experimental results about the coalescence stability of emulsions stabilized by different emulsifiers. To make this comparison quantitative, we should use the appropriate physico-chemical characteristic of the emulsion stability which depends as little as possible on the experimental method and protocol used. In our studies with proteins and LMM surfactants, we demonstrated that such a characteristic could be the critical osmotic pressure leading to emulsion destabilization, P_{OSM}^{CR}, which can be determined by centrifugation and some other experimental methods.[41,46] Higher values of P_{OSM}^{CR} correspond to more stable emulsions and *vice versa*.

The main advantages of using P_{OSM}^{CR} for characterizing emulsion stability are:[41,46] (1) it has a clear physico-chemical definition and meaning, (2) it could be determined precisely by several methods, the most convenient of them being emulsion centrifugation, and (3) it is a characteristic of the emulsion itself, so the experimental result should not depend on the specific method used if the experiments are properly conducted. The specific technical protocol, several experimental checks to verify the centrifugation method used by us, experimental results with various systems and detailed physico-chemical interpretation of these results are presented in ref. 41–46 and will not be reproduced here. We present below only the final results for P_{OSM}^{CR}, needed for the comparison with the particle-stabilized emulsions.

Systematic experiments with emulsions stabilized by proteins or LMM surfactants showed that the emulsion coalescence stability rapidly decreases with the increase of the mean drop radius, R_{32}.[41,46] The experiments showed that for approximate estimates, one can assume that the critical pressure for emulsion destabilization is proportional to the inverse drop radius, $P_{OSM}^{CR} \propto 1/R$.[41,46] Therefore, the proper comparison of the stability of various emulsions would be incorrect, unless emulsions containing drops of similar size are studied, or the drop-size effect is taken into account. Because we have not found experimental data allowing direct comparison of the emulsion stability for different types of emulsifiers (including solid particles) in the literature, below we use data from several independent studies. To account approximately for the drop-size effect, the comparison is made by scaling the critical pressure for emulsion destabilization with the inverse drop radius, *i.e.* the values of the product $R_{32}P_{OSM}^{CR}$ are compared.

By centrifugation we showed[44] that hexadecane-in-water emulsions, stabilized by typical individual LMM surfactants

of concentration well above their CMC and containing droplets with size $R_{32} \approx 3$ μm, exhibit critical pressures for emulsion destabilization between *ca.* 20 and 60 kPa. For example, for the nonionic surfactant Brij 58 we measured $P_{OSM}^{CR} \approx 60$ kPa, and for the anionic surfactant SDS $P_{OSM}^{CR} \approx 25$ kPa. By preparing appropriate surfactant mixtures, we obtained more stable emulsions (at a similar drop size) with $P_{OSM}^{CR} \geq 100$ kPa. Similar values were obtained when studying oil-in-water emulsions stabilized by polymers, such as PVA ($P_{OSM}^{CR} \approx 30$ kPa)[44] and globular proteins ($P_{OSM}^{CR} \approx 30$ kPa),[103] with mean drop radius $R_{32} \approx 8$ μm.[44,103] Note that no specific efforts were made to maximize the emulsion stability in these studies, except that the surfactant mixtures that were designed to ensure high stability. Thus we could conclude that for surfactant and protein-stabilized emulsions, containing droplets with radius between 1 and 5 μm, the emulsion destabilization occurs typically in the range between 20 and 100 kPa, and the product $R_{32}P_{OSM}^{CR}$ is in the range 0.1 to 0.3 Pa m. For the optimized surfactant mixtures $R_{32}P_{OSM}^{CR} > 0.3$; the exact value is unknown because the respective emulsions did not decay in the centrifugation tests performed.

In an independent study, van Aken and Zoet[104] assessed the stability of sunflower oil-in-water emulsions containing submicrometer droplets stabilized by SDS or protein. They found that the emulsions containing drops with $R_{32} \approx 0.65$ μm and stabilized by 0.5 wt% protein mixture (whey protein isolate) remained stable after centrifugation at relative centrifugal field RCF $= g_C/g \approx 10^5$ (g_C is the centrifugal acceleration, g is the acceleration of gravity). By using the technical description of the centrifugation procedure used in ref. 104, we estimated that this RCF corresponded to $P_{OSM}^{CR} \approx 300$ kPa, *i.e.* the product $R_{32}P_{OSM}^{CR} \approx 0.3$ Pa m. Similarly, for the emulsions stabilized by SDS with concentration $C > 0.5$ wt% (drop radius of 0.38 μm), $P_{OSM}^{CR} > 300$ kPa can be estimated from the reported experimental data, which corresponds to $R_{32}P_{OSM}^{CR} > 0.12$ Pa m. Thus we see that the results obtained in ref. 104 agree well with the results from ref. 44 and 103, if the drop-size effect on emulsion stability is taken into account.

Quantitative experimental results for the coalescence stability of particle-containing emulsions are reported in several papers only.[30,105] In the paper by Kruglyakov *et al.*[105] a specially designed method was used to measure the critical capillary pressure (similar in meaning and magnitude to the critical osmotic pressure used in the centrifugation studies), which leads to destabilization of a decane-in-water emulsion stabilized by 1% Ludox particles. The experimentally determined critical pressure was around 3 kPa only, whereas a much higher value was expected from theory.[105] Even if we assume that the drop radius in this study was as large as $R_{32} \approx 20$ μm (it was not reported in the paper), this would correspond to $R_{32}P_{OSM}^{CR} \approx 0.06$ Pa m. Thus we see that these particle-stabilized emulsions were not particularly stable compared to the published results for typical LMM surfactants and polymers.

In another study,[30] water-in-oil emulsions containing drops with $R_{32} \approx 0.28$ μm and stabilized by silica particles were studied by ultracentrifugation. The critical acceleration field for destabilization of emulsions containing 1 wt% particles was RCF $\approx 2 \times 10^4$, from which we estimated the corresponding critical pressure $P_{OSM}^{CR} \approx 300$ kPa and the respective product $R_{32}P_{OSM}^{CR} \approx 0.08$ Pa m. Therefore, the emulsion stability determined in these experiments was lower than the stability ensured by the good surfactant emulsifiers.

One can conclude from the above comparison that the available experimental data do not support the hypothesis that the particle-stabilized emulsions are exceptionally stable with respect to drop–drop coalescence, as compared to the typical surfactant- and protein-stabilized emulsions. Obviously, further systematic experiments with particle-stabilized emulsions are deserved to clarify this issue.

3.1.2 Mechanical equilibrium of liquid films—role of the disjoining and capillary pressures. The overall coalescence stability of emulsions and foams is determined by the stability of the thin liquid films formed between the neighboring drops/bubbles.[75,76,82,106,107] In the systems stabilized by ionic surfactants, the film stability is often described reasonably well by accounting for the van der Waals and electrostatic interactions (DLVO theory).[82,107–110] The adsorbed nonionic surfactants and flexible polymer chains are usually described as creating steric repulsion between the film surfaces, which arises from the overlapping of the hydrophilic heads (or chains) of the surfactant (polymer) in the film interior.[80,111–115] In the case of charged flexible polymers, both electrostatic and steric interactions are operative. The case of globular polymers (such as the globular proteins) is discussed in section 3.1.5 below.

It is worthwhile noting that both the electrostatic and steric interactions could be explained in terms of an excess of osmotic pressure of the water in the thin film. This excess is created by a higher concentration of counterions (for the ionic surfactants) or by a higher concentration of hydrophilic segments (for the nonionic surfactants and polymers) in the middle of the film, as compared to these concentrations in the bulk continuous phase, Fig. 6A and B.[80] This excess of osmotic pressure acts to "suck in" water from the bulk phase, thus creating an effective repulsion between the film surfaces. Therefore, for such a thin film to be in mechanical equilibrium, the repulsive surface forces in the film should be counterbalanced by external forces pushing the film surfaces against each other, Fig. 6C. The theoretical analysis show that the condition for mechanical equilibrium in the film is[75,106,116]

$$\Pi(h) = P_C \qquad (23)$$

where $\Pi(h)$ is the disjoining pressure (surface force per unit area) and P_C is the capillary pressure of the curved menisci around the film, where the surface forces are negligible.

The main advantage of this mechanical balance is that it involves $\Pi(h)$, which is an appropriate theoretical quantity that could be calculated for an imaginary film with infinite radius, without considering the specific configuration of the real system. On the other hand, P_C depends on the specific configuration (*e.g.* on the drop size, volume fraction of the drops in the emulsions, height of the emulsion column *etc.*), but is often amenable to experimental determination[106–117] or to an approximate theoretical estimate for the real emulsions.[41,46,118] Therefore, eqn (23) provides a convenient link between the theoretical predictions for the stability of single films and the stability of the overall emulsion. The emulsion

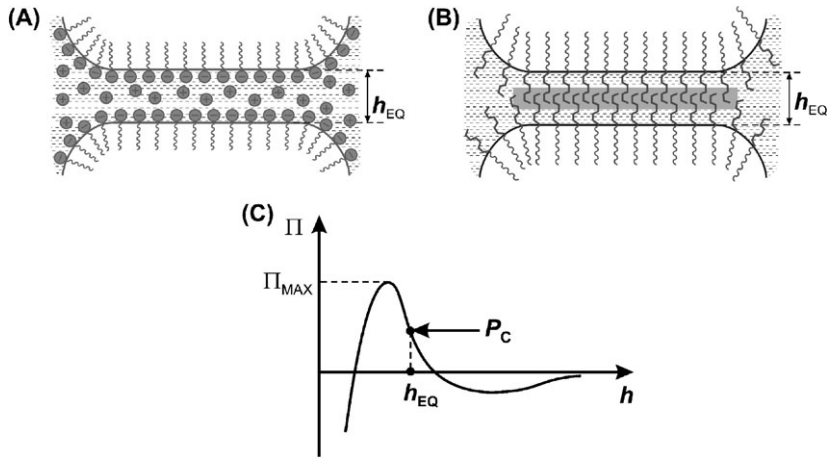

Fig. 6 Schematic presentation of the structure of the adsorption layers and the respective mode of emulsion film stabilization by (A) ionic surfactants, and (B) nonionic surfactants. (C) Schematic presentation of disjoining pressure isotherm—P_C is the capillary pressure squeezing the liquid from the film, h_{EQ} is the equilibrium film thickness, and Π_{MAX} is the maximum in the isotherm.

stability analysis is usually based[42,46,118,119] on comparing the capillary pressure in the emulsion, P_C, with the maximum of the dependence $\Pi(h)$, which is denoted hereafter by Π_{MAX}, see Fig. 6C.

For example, the capillary pressure of the drops in a concentrated emulsion column, subject to gravity or homogeneous centrifugal field can be estimated by the expression:[119]

$$P_C(z) \approx \sigma/R + \Delta\rho g_C z \qquad (24)$$

where R is the drop radius, σ is the interfacial tension, $\Delta\rho$ is the mass density difference between the drops and continuous phase, g_C is the acceleration (centrifugal or gravity), $0 \leq z \leq H$ is the vertical coordinate of the drop in the emulsion column and H is the total height of this column. One sees from eqn (24) that the capillary pressure of the drops is highest at the top of the emulsion column, so that the drop coalescence would start there once the centrifugal acceleration, g_C, or the height of the emulsion column increase up to the moment at which $P_C(H)$ becomes higher than Π_{MAX}.

A more detailed description of the various types of surface forces operating in liquid films stabilized by LMM surfactants and polymers, and of the relations between the capillary and osmotic pressures in emulsions and foams, can be found in the literature.[75,76,80–82,106,107,118–123]

3.1.3 Capillary mechanism of emulsion stabilization by solid particles. The theoretical approach for the description of the stabilization of liquid films by solid particles is based on consideration of the shape of the fluid menisci formed between the neighboring particles,[19,20] see Fig. 7. Because this analysis is entirely based on the theory of capillarity we call this mechanism ''capillary stabilization'' of the films by particles. Very often another term, ''steric stabilization by particles'', is used in the literature. We refrain from using this term in our work for two main reasons:

(1) The term ''capillary stabilization'' shows directly which is the physical phenomenon governing the stability of particle-stabilized films, namely the capillary shape of the menisci between the solid particles. In contrast, the term ''steric stabilization'' emphasizes the direct contact between the solid particles in the film without indicating anything about the actual mechanism of the stability–instability transition. Furthermore, as explained below, the particle-stabilized films rupture when the fluid menisci at the two opposite film surfaces touch each other, without necessarily changing the actual contacts between the solid particles. Therefore, the term ''steric stabilization'' drives the attention away from the main physical phenomenon, controlling the stability of these systems. It is particularly inappropriate when films containing particle monolayers (Fig. 7) are considered, which seems to be often the case in the real systems.[4,39]

(2) The mechanism of stabilization by particles is conceptually different from that by nonionic surfactants and polymers, for which the term ''steric stabilization'' has been widely accepted for years.[80,82,106] To avoid confusion, we use the term ''steric stabilization'' for surfactants and polymers only.

The conceptual frame of the capillary mechanism of film stabilization is fairly simple, although the technical difficulties in the numerical calculations are significant. For clarity, we describe below the case of liquid films, stabilized by spherical particles, in the absence of surfactants. The effects of particle shape and surfactants could be easily incorporated at a qualitative and at a semi-quantitative level, but we refrain from doing this to keep the explanations simple and the focus clear.

For a liquid film to rupture, the two opposite fluid surfaces must approach each other to the so-called ''critical film thickness'', h_{CR}, at which the film spontaneously thins down and ruptures under the action of attractive van der Waals forces.[124,125] Typically, h_{CR} is of the order of several nanometers to 30 nm.[125] Because the particles have certain hydrophobicity, characterized by their three-phase contact angle (Fig. 7), the fluid interfaces in the film acquire a certain shape which depends on several factors. For regular arrays of spheres, the shape of the fluid interfaces depends on: capillary pressure across the fluid interface, P_C; particle radius, a; three-phase contact angle, α; oil–water interfacial tension, σ; inter-particle distance, b; and whether the particles form a

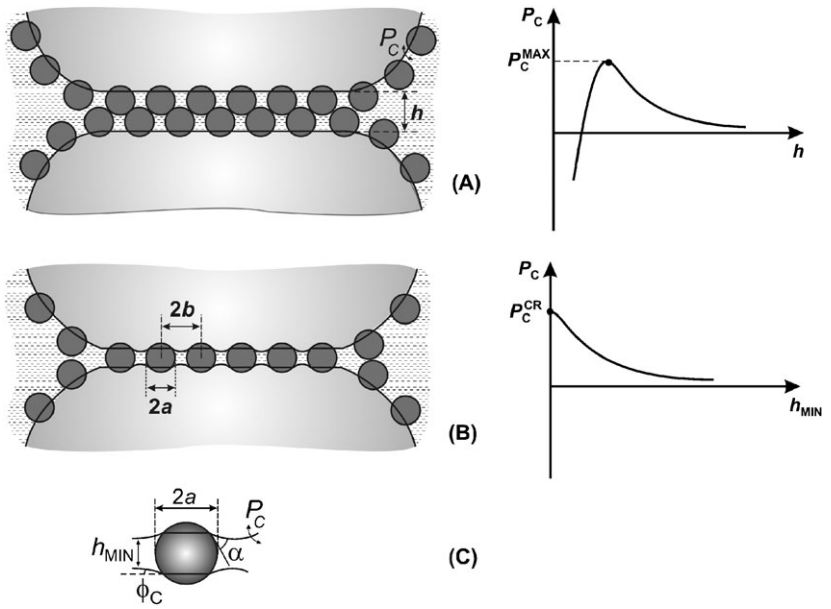

Fig. 7 Schematic presentation of the structure of particle bilayer (A), and monolayer (B), stabilizing an emulsion film. The respective shapes of the dependence "capillary pressure *vs.* film thickness" are also shown. In (C) the curved shape of the meniscus around a particle in the monolayer is shown and the contact angle, α, the slope angle at the contact line, ϕ_C, and the minimal film thickness, h_{MIN}, are indicated. Note that in the case of a bilayer (A) the film ruptures when the capillary pressure (squeezing the liquid from the film) becomes higher than P_C^{MAX}, whereas in the case of a monolayer (B) the film ruptures when the minimal film thickness, h_{MIN}, becomes equal to the critical thickness for film rupture, $h_{CR} \approx 0$.

monolayer or bilayer inside the film (both configurations are observed experimentally),[39,126] see Fig. 7. Therefore, the theoretical problem for the film stability consists of determining the dependence of the menisci shape and of the respective minimal distance between the two fluid surfaces of the film, h_{MIN}, on the capillary pressure, P_C (all remaining parameters are considered as fixed). In these calculations, P_C is considered as external free variable which depends on the overall configuration of the emulsion (section 3.1.2).

Two different scenarios for film rupture are theoretically predicted:[19,20]

(1) The first scenario is typical for the films containing a single layer of particles, Fig. 7B. In this case, h_{MIN} is a monotonically decreasing function of P_C and one should determine the critical capillary pressure, P_C^{CR}, which squeezes the two fluid surfaces of the film down to thickness $h_{MIN}(P_C^{CR}) = h_{CR}$. In this scenario, P_C^{CR} is the maximum capillary pressure that could be resisted by the film, before it ruptures.

(2) In the second scenario, typical for the films stabilized by a bilayer of particles (Fig. 7A), P_C passes through a maximum (P_C^{MAX}) before the condition $h_{MIN} = h_{CR}$ is reached. This means that, after the external capillary pressure P_C reaches P^{MAX}, the subsequent film thinning down to h_{CR} is spontaneous because the film is mechanically unstable. In this scenario, the value of P_C^{MAX} corresponds to the maximum pressure that could be resisted by the film before it ruptures.

The research problem for finding the dependence $h_{MIN}(P_C)$ was first formulated and solved numerically with reasonable approximations in ref. 19. Scenario 1 was considered in detail, and the numerical results obtained were in qualitative agreement with all main experimental trends known at that time for particle-stabilized emulsions. In particular, the calculations predicted that: (1) P_C^{CR} is proportional to $1/a$, *i.e.* the smaller particles give more stable films, (2) P_C^{CR} rapidly decreases upon an increase of the interparticle distance in the adsorption layers, and (3) lower particle contact angles correspond to higher P_C^{CR}, *i.e.* to more stable films (the films are unstable for $\alpha \geq 90^\circ$). The effect of the possible contact-angle hysteresis was also analyzed and found to enhance film stability.

The numerical results for P_C^{CR} obtained in ref. 19 could be represented by the following scaling formula:

$$P_C^{CR} \approx k(\sigma/a) \text{ (monolayers)} \qquad (25)$$

where $k(\alpha,b/a)$ is a dimensionless parameter which is calculated numerically and depends on the particle contact angle and the mean interparticle distance (see also eqn (29) below). The calculations showed[19] that k could be of the order of 10 for closely-packed particles and small angles, α. This high value of k corresponds to extremely stable films—the predicted value of P_C^{CR} corresponds to the radius of curvature of the fluid interfaces, which is an order of magnitude smaller than the particle radius! Even higher pressures for film rupture were predicted in ref. 19 for films stabilized by close-packed particle bilayers (scenario 2). Based on these theoretical predictions, it was speculated in ref. 19 that the rupture of the particle-stabilized films in the real systems could occur only through "cracks", "vacancies" or other defects in the particle arrays, with the very probable formation of a particle monolayer bridging the two film surfaces (Fig. 7B, scenario 1) as an intermediate stage between the particle bilayer and film rupture. Subsequent optical observations confirmed these speculations, showing that usually the films spontaneously thin down until a monolayer of particles is formed.[39,127–130] Furthermore, this particle monolayer is usually not homogeneous, containing film areas free of particles due to the

important effect of lateral capillary forces, which are discussed below.

Numerical calculations of the dependence $P_C(h_{MIN})$ for particle bilayers (scenario 2, Fig. 7A) were presented in ref. 20 and 105. Kruglyakov *et al.*[20,105] proposed the following expression for the maximal capillary pressure:

$$P_C^{MAX} = k \cos \alpha(\sigma/a) \text{ (dense bilayers)} \quad (26)$$

where $k \approx 1.73$ was proposed for a close-packed particle bilayer. In a very detailed study of the fluid penetration into porous medium composed of spherical particles, Mason and Morrow[131] showed theoretically that P_C^{MAX} is obtained at $\alpha + \phi_C > 90^\circ$ (not at $\alpha + \phi_C = 90^\circ$, as supposed in ref. 20 and 105), and the following, much better approximation for P_{MAX} was derived:[39,131]

$$P_C^{MAX} = \frac{2\sqrt{1-(3/4)\sin^2\alpha}}{\{2/\sqrt{3} - \sin[\alpha + \arccos((\sqrt{3}/2)\sin\alpha)]\}}(\sigma/a)$$

(dense bilayers) (27)

Eqn (27) predicts values for P_C^{MAX}, which are an order of magnitude higher than the values predicted by eqn (26), and are in semi-quantitative agreement with the calculations based on the model in ref. 19 for the contact angles of major interest, $0 \leq \alpha \leq 120^\circ$ (the difference is around or lower than 50%).

As discussed in ref. 19, 39 and 131, the magnitude of P_C^{MAX} could be estimated by considering the pressure needed for pushing the liquid menisci through pores with a diameter comparable to the cross-section of the gaps formed between the neighboring particles in the film—this analogy is very helpful, because it allows one to estimate the magnitude of P_C^{MAX} for non-regular particle arrays by taking the biggest gap between the particles in the film as the characteristic "pore" size (see ref. 131 and the further discussion below).

As explained already, all theoretical models predict an exceptionally high stability of the films containing regular arrays of close-packed particles (at $\alpha < 90^\circ$). In fact, according to this prediction, such films should not be destroyed under realistic conditions and this is obviously in contradiction with the available experimental results, see section 3.1.1. Therefore, the theoretical models capture well the main qualitative trends, but predict orders of magnitude higher pressures for emulsion destabilization, in comparison with the experimentally determined ones. The main reason for this quantitative discrepancy is the implicit assumption made in all models that the particles are homogeneously distributed in the films. This assumption strongly underestimates the size of the biggest "pores", formed in the particle layers. These biggest "pores" are crucial for the film stability because the menisci could protrude through these pores (thus causing a film rupture) at much lower capillary pressures than those predicted for homogeneously distributed particles with the same average surface coverage, Fig. 8.

As clarified by the optical observations, there are three main reasons for the formation of inhomogeneous particle layers in the foam and emulsion films:

First, the long-range electrostatic repulsion between the particles attached to single interfaces leads to formation of adsorption layers in which the particles are often not packed closely.[23,38,39,132] Note that no capillary attractive force appears between submicrometer spherical particles adsorbed on single fluid interface [21] unless the particle surfaces are corrugated or inhomogeneous so that perturbations of the fluid interface from its equilibrium shape (in the absence of particles) are created.[133,134]

Second, very strong lateral capillary forces appear between the particles captured in the emulsion films, when the menisci between the particles become curved (*i.e.* the capillary pressure needed to induce film rupture necessarily generates lateral capillary forces).[21,135,136] These lateral forces are attractive and lead to condensation of the particles in close-packed patches, thus creating spots in the films which are free of particles.[129,130] The theory predicts that the capillary forces of this type (between particles captured in liquid film) are of the order of:[21,136]

$$F_{CF} \sim \sigma a + P_C a^2 \quad (28)$$

and they usually prevail over all other types of interparticle forces (electrostatic, van der Waals *etc.*), if present. In addition, when the particle adsorption monolayers on the surfaces of two drops touch each other in the process of film formation, a lateral mechanical force appears between the touching particles which facilitates their rearrangement and the formation of particle monolayer in the film—this effect was observed and theoretically analyzed in ref. 39.

Third, the emulsion destabilization almost always involves some deformation of the drops (*e.g.* due to emulsion flow, or to emulsion compaction in gravity or centrifugal field) which leads to expansion of the drop surfaces, thus creating spots deprived of particles. These spots are the "weakest points" where the film rupture may occur. As explained after eqn (27), the capillary pressure leading to film rupture for such irregular particle configurations could be approximately estimated to be of the order of (or lower than) $P_C^{MAX} \sim \sigma/R_P$, where R_P is the characteristic size of the biggest pore in the particle layer stabilizing the film. Note that R_P could be orders of magnitude larger than the particle radius, a, which explains why the experimental pressures leading to emulsion destruction are lower than those predicted theoretically for regular particle arrays.

3.1.4 Capillary component of the disjoining pressure in particle-stabilized films. It is useful in some considerations (*e.g.* in mechanical balances, such as eqn (23)) to deal with a disjoining pressure component, $\Pi_{CAP}(h_{MIN})$, that can be associated with the capillary stabilization of the liquid films

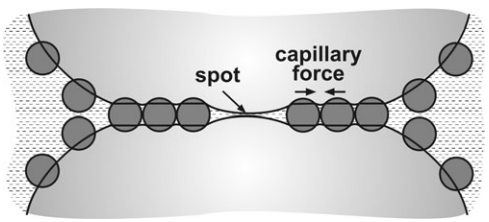

Fig. 8 Schematic presentation of the spot formation inside film stabilized by solid particles, as a result of lateral capillary forces.

by particles. By making a rigorous balance of the normal capillary forces acting on a solid particle in liquid film (normalized by the area occupied by a particle), the following expression for Π_{CAP} was derived[19] for a regular array of particles:

$$\Pi_{CAP}(h_{MIN}) = 2\sigma \frac{a\sin(\phi_C + \alpha)}{b^2 - a^2\sin^2(\phi_C + \alpha)} \sin\phi_C \qquad (29)$$

where ϕ_C is the meniscus slope angle at the contact line of the particle, Fig. 7C. This slope angle is related to the minimal film thickness, h_{MIN}, however the function $\phi_C(h_{MIN})$ can be found only by numerical solution of the Laplace equation of capillarity.[19,20] Therefore, eqn (29) relates the disjoining pressure and the film thickness in a non-explicit way, thus requiring numerical calculations to find the function $\Pi_{CAP}(h_{MIN})$.

Note that eqn (29) is valid for both a monolayer and bilayer of particles, and only h_{MIN} differs in these two cases—for example, for geometrical consideration one can find that h_{MIN} for a close packed bilayer of particles is larger by $\approx 1.63a$, as compared to h_{MIN} for a close-packed monolayer of particles at the same capillary/disjoining pressure.

As shown in ref. 19, the condition for mechanical equilibrium, $P_C = \Pi_{CAP}$ (*cf.* eqn (23)), is identically satisfied with the above definition of Π_{CAP}, *i.e.* at a phenomenological level we have a complete analogy between the films stabilized by particles and by the other emulsifiers. This also means that the maximum capillary pressure P_C^{MAX} in the capillary models (Fig. 7A) is equivalent to the disjoining pressure barrier Π_{MAX} (Fig. 6C).

3.1.5 Mechanisms of emulsion stabilization by globular proteins. In this section we briefly discuss the film stabilization by globular proteins. It was recognized years ago that the lateral capillary forces between protein molecules captured in liquid films could play an important role for the protein–protein interactions and are a key factor in the formation of ordered protein structures.[21,136–138] In an independent study[46,47] we showed that the formation of emulsions in the presence of globular proteins, at high electrolyte concentrations and/or around the isolectric point (IEP) of the protein, could be described by considering the globular protein molecules as small nanoparticles (without any specifics needed). On the other hand, the stability of oil-in-water emulsions at low electrolyte concentrations, $C_{EL} < 50$ mM and pH away from the IEP of the used globular protein (β-lactoglobulin, BLG), was successfully explained by considering the electrostatic and van der Waals interactions, just as in the case of ionic surfactants.[42,46,47]

Reviewing all these results, we can conclude that during emulsification and with respect to the short-term stability of emulsions, the proteins may behave like ionic surfactants or like nanoparticles, depending on the conditions.[46,47] On the other hand, the long-term stability of protein emulsions changes in a very specific way after heating or aging of the emulsion, due to the possibility of formation of intermolecular bonds, *i.e.* the proteins exhibit their own specific features upon such treatments.[43] For further discussion of these features, see ref. 46 and 47.

3.2 Ostwald ripening

In the Ostwald ripening process, the small drops/bubbles gradually diminish and disappear, at the expense of the growth of the bigger drops and bubbles. In this section we briefly describe the basic mechanism by which the solid particles can stabilize emulsions and foams with respect to this process.

The driving force for the Ostwald ripening is the difference in the chemical potentials of the molecules in the small and in the large drops, which in its turn is caused by the dependence of the capillary pressure on the drop size, $P_C(R)$. For this process to occur, the molecules of the dispersed phase should have some solubility in the continuous phase, thus allowing a transport through molecular diffusion of material from the small toward the large drops. The process is very important for foams (due to the relatively high solubility of gases) and for emulsions containing oils with small molecules, especially those with high polarity and polarizability (hexane, benzene, xylene, short-chain PDMS), because of their noticeable solubility in water. The process could be facilitated by surfactant micelles, which may act as reservoirs and carriers of the dissolved molecules.

A detailed theoretical model for description of the rate of the Ostwald ripening process was developed by Lifshitz and Slyozov[139] and Wagner[140] (the so-called "LSW theory"). After sufficiently long times, the LSW theory predicts a quasi-stationary regime in which the rate of changing the drop size is described by the expression:

$$v = \frac{dR_N^3}{dt} = \frac{4}{9}\beta D S_\infty \qquad (30)$$

where R_N is the number averaged drop radius, D is the diffusion coefficient of the dissolved molecules, and S_∞ is the bulk solubility of the dispersed phase in the continuous phase. The parameter β is defined as:

$$\beta = \frac{2\sigma V_M}{k_B T} \qquad (31)$$

where V_M is molecular volume of the dispersed phase. These equations predict that the rate of ripening depends mostly on the bulk solubility of the dispersed phase, the interfacial tension and the drop/bubble size.

The Ostwald ripening in emulsions and foams, stabilized by surfactants and proteins, was widely studied in the literature.[141–149] In the context of the current discussion, the main experimental observations can be summarized as follows:

(1) The LMM surfactants significantly decrease the interfacial tension, thus reducing the driving force of the process. However, the micelles formed above the critical micelle concentration (CMC) increase the solubility of the dispersed phase, S_∞, thus facilitating the process. Due to the relatively fast adsorption/desorption of the typical surfactants, σ can be considered as constant throughout the entire process, equal to the equilibrium interfacial tension of the surfactant solution.

(2) The equilibrium interfacial tension for protein-stabilized emulsions and foams is higher than the interfacial tension for LMM surfactants, which initially leads to higher capillary pressure and faster ripening (with all other conditions fixed). However, due to the high desorption energy of the protein

molecules, they desorb slowly. As a result, the shrinking of the small drops and bubbles leads to increased adsorption of protein on the drop/bubble surfaces, thus reducing the interfacial tension and slowing down the ripening process. No complete arrest of the Ostwald ripening process has been reported for proteins.

(3) Particles are able to completely arrest the Ostwald ripening in foams and emulsions.[5,6,149,150] This feature is particularly important for some food foams, in which the solid particles (fat globules, mineral particles, or ice crystals) are essential for ensuring long-term stability of commercial products, such as mousses and ice-creams.

The available experimental results suggest that the possibility for a complete arrest of the Ostwald ripening by solid particles is related to their exceptionally high desorption energy.[34–36] For spherical particle with radius a, the energy for particle desorption from a fluid interface with interfacial tension σ, is:

$$W = \pi a^2 \sigma (1 - |\cos \alpha|)^2 \qquad (32)$$

where α is the contact angle of the particle, measured through the aqueous phase. This formula shows that the adsorption energy is proportional to the particle area, $W \propto a^2$, and that maximal adsorption energy, $W = \pi a^2 \sigma$ is obtained at $\alpha = 90^\circ$. The numerical estimates for $\sigma = 30$ mN m^{-1} and $\alpha = 90^\circ$ gives $W \approx 10^2\ k_B T$, $10^4 k_B T$ and $10^6 k_B T$ for particles with a radius of 1, 10 and 100 nm respectively. Because this energy enters in the exponential factor, when considering the kinetic constant of particle desorption[21] all particles with radius larger than several nanometers adsorb virtually irreversibly on the fluid interfaces (unless the contact angle is very close to 0 or 180°).

It is worthwhile mentioning that two different interfacial tensions should be distinguished when considering particle-stabilized systems. The first one (denoted by σ throughout the paper) is the interfacial tension of the oil–water interface, which is not covered by particles. This interfacial tension does not depend on the particle adsorption because it is determined by the properties of the contacting oil and water phases only (and of the surfactant, if present). Note that even for close-packed, *viz*. a compressed or even collapsed layer of particles, the interfacial tension of the menisci between the particles remains the same as that of the bare oil–water interface. The second tension (denoted by σ_A below) is the macroscopic, apparent interfacial tension of the interface, which is dependent on the surface coverage by particles. It is this interfacial tension, σ_A, that appears in all macroscopic mechanical balances involving the drops and bubbles whose surfaces are covered by particles. For example, σ_A should be used in all balances at the structural level of drops and bubbles (*i.e*. in eqn (5) and (6)). In contrast, σ should be used in all microscopic considerations of the menisci around the particles in the adsorption layers and in the films. These two interfacial tensions are interrelated through the two-dimensional surface pressure of the particle layer, $\Pi_S(\Gamma)$, which can be determined experimentally:

$$\sigma_A = \sigma - \Pi_S(\Gamma) \qquad (33)$$

Systematic experiments for determination of the dependence $\Pi_S(\Gamma)$ for particle monolayers were performed by using Langmuir trough and pendant drops.[23,24,37,66] These experiments showed that the collapse of the particle monolayers, on both the air–water and octane–water interfaces, occurs through folding and corrugations of the interface.[23,24,37,66] For the octane–water interface, these processes occur when Π_S approaches σ.[23,24,66] In other words, upon compression and collapse of the particle layers the apparent interfacial tension, σ_A, and the drop capillary pressure, $P_C = 2\sigma_A/R$, approach zero so that the driving force for the Ostwald ripening disappears.

The requirement to have self-consistent macroscopic and microscopic descriptions of the curved particle monolayers on the surface of such drops leads to the conclusion that the local radii of curvature of the real menisci between the particles should be equal in magnitude and opposite in sign to cancel each other, that is, these local menisci have zero mean curvature, $P_C = \sigma(1/R_1 + 1/R_2) \approx 0$, see Fig. 9. A basic theoretical consideration of this effect can be found in ref. 151. Another possibility for obtaining a vanishingly small mean curvature of the fluid interface was recently described by Abkarian *et al*.[150] who showed experimentally and theoretically that at appropriate particle-to-bubble size ratio, the bubbles spontaneously acquire faceted polyhedral shapes with planar fluid interfaces at the walls. (The experiments[66] showed that the possible effect of the monolayer bending moment is not detectable and is, therefore, omitted in the current consideration).

The protein molecules are also known to have high adsorption/desorption energies and they are often considered as irreversibly adsorbing on air–water and oil–water interfaces.[152–155] However, the experimental studies of the $\Pi_S(\Gamma)$ isotherms for protein layers showed that the collapse pressure of these layers is lower than the interfacial tension of the bare oil–water (or air–water) interface.[154,156] This result evidences that, although the desorption of the protein molecules is rather slow when considering the thermal energy and relatively small compressions of the layers, the protein molecules can desorb when compressed under high surface pressures. Indeed, direct experiments showed that the rate of desorption of protein molecules can be measured and it significantly decreases while increasing the molecular diameter.[154]

On the basis of all these results one can conclude that the main differences between low-molecular-mass surfactants, proteins and solid particles, with respect to Ostwald ripening, can be explained by the different size of the respective entities, which in turn results in different desorption rates—relatively high for surfactants, intermediate for proteins and negligible for particles. The complete arrest of Ostwald ripening by particles is thus explained by the fact that the compression of particle layers, upon shrinking of the drop/bubble surface in the process of ripening, diminishes the macroscopic (apparent) interfacial tension, $\sigma_A \to 0$ (by creating micro-configurations with zero mean curvature of the fluid interface between the particles), and thus eliminates the driving force of the process. This analysis suggests that very small, non-aggregated nanoparticles with a radius comparable to that of protein molecules

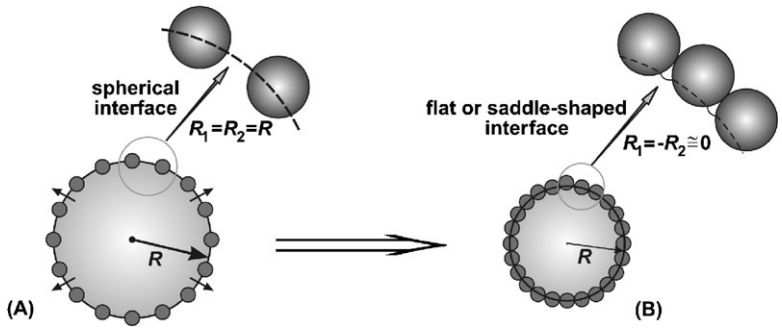

Fig. 9 Schematic presentation of the mechanism of Ostwald ripening arrest by solid particles. When the particles form a complete jammed monolayer due to their very high desorption energy, the diffusion of the internal fluid phase to the continuous phase leads to an inward bending of the fluid interface between the particles, so that the capillary pressure driving the Ostwald ripening disappears.

might be unable to completely arrest the Ostwald ripening, whereas properly structured molecular aggregates on the drop/bubble surface might be able to accomplish this task.

4. Conclusions

The performed comparison of the various types of emulsifiers shows that some non-obvious similarities can be outlined in the cases in which the description of the system can be performed at the phenomenological level. Appropriate examples are the mass-balance equations, used to predict the mean drop size in the process of emulsification, which are equally applicable (with simple modifications) to all types of emulsifiers, see eqn (1)–(13) and (23) and Fig. 1 and 3.

The differences between the emulsifiers are significant in the cases in which the detailed mechanisms of adsorption and film stabilization are important. The main specific features of the solid particles which control their behavior during emulsification and emulsion stabilization are: the high barrier to particle adsorption, high desorption energy and strong capillary forces between particles trapped in liquid films, which all stem from the relatively large particle size (as compared to the size of surfactant and protein molecules). This important size effect suggests that the small nanoparticles with diameter of 1–5 nm could exhibit behavior closer to globular proteins (as compared to the bigger solid particles), due to the comparable size and desorption energy.

The mechanism of stabilization of liquid films by solid particles (in foams or emulsions) is based on capillary phenomena. The two different scenarios of film rupture (for films stabilized by a monolayer or bilayer of solid particles) are briefly presented and the respective capillary pressures for film rupture are discussed. Although the exact calculations of the shape of the menisci between the particles (needed to calculate film stability) are rather difficult, several simple expressions can be used for approximate estimates. The concept of the capillary component of the disjoining pressure, originating from the capillary mechanism of film stabilization by solid particles, is explained.

The performed comparison of the available results for the coalescence stability of various emulsions unexpectedly revealed that the hypothesis for exceptionally high stability of the particle-stabilized emulsions is not supported by the experimental data. On the other hand, the particles are able to completely arrest the process of Ostwald ripening in foams and emulsions, and this effect can be easily explained with the high desorption energy of the particles and the resulting capillary effects.

Most of the conclusions outlined above are equally applicable to both particle-stabilized emulsions and foams. It would be interesting to see whether the approach based on comparing the properties of the different types of emulsifiers could be extended further to provide useful results for other properties of the particle-stabilized emulsions (and foams), such as their rheological and optical properties, and the conditions for phase inversion. This extension is left for a subsequent study.

Notation

Capital Latin letters

A—dimensionless constants appearing in the equations for the drop diameter, d

A_1—eqn (5)

A_2—eqn (6)

A_H—Hamaker constant

C—concentration

C_{EL}—electrolyte concentration

C_{INI}—initial emulsifier concentration

C_P—concentration of particles

C_{SER}—surfactant concentration left in the aqueous phase after emulsification

D—diffusion coefficient of the dissolved molecules, eqn (30)

F—force

F—interaction force between particle and oil–water interface

F_{MAX}—height of the electrostatic barrier between particle and drop

F_T—hydrodynamic force pushing particle to drop surface in turbulent flow, eqn (19)

F_S—hydrodynamic force pushing particle to drop surface in simple shear flow, eqn (20)

F_{CF}—lateral capillary force between particles trapped in liquid film, eqn (28)

H—height of emulsion column

I—ionic strength

Q—particle charge, eqn (22)

P—pressure

P_C—capillary pressure

P_C^{CR}—maximum capillary pressure that could be resisted by the film before it ruptures (monolayer), Fig. 7B

P_C^{MAX}—maximum capillary pressure that could be resisted by the film before it ruptures (bilayer), Fig. 7A

$\langle \Delta P_T(d) \rangle$—statistically averaged fluctuations in the dynamic turbulent pressure between two points separated at distance, d, from each other

P_{OSM}—osmotic pressure of emulsion

P_{OSM}^{CR}—critical osmotic pressure, leading to emulsion destabilization

R—drop radius

R_{32}—experimentally measured mean volume–surface radius

R_p—characteristic radius of the biggest pore in the particle layer

R_N—number average drop radius

S_∞—solubility of the dispersed phase in the continuous medium, eqn (30)

T—temperature

V—volume

V_M—molecular volume of dispersed phase

U—characteristic velocity of the flow

W—interaction energy between particle and fluid surface, eqn (21)

W_{MAX}—maximal energy of repulsion

Small Latin letters

a—particle radius

b—interparticle distance in the layer, Fig. 7

d—drop diameter

d_D—maximum diameter of stable drops in turbulent flow, eqn (6) (Davies,[62] inertial regime)

d_K—maximum diameter of stable drops at negligible effect of the drop viscosity, eqn (5) (Kolmogorov–Hinze,[59,60] inertial regime)

d_{KI}—group $(\varepsilon^{-2/5}\sigma^{3/5}\rho_C{}^{-3/5})$ with dimension of length, eqn (5)

d_{32}—experimentally measured mean volume–surface diameter

d_{V95}—experimentally measured maximum drop diameter, 95% by volume

e—elementary electrical charge

g—gravity acceleration

g_C—centrifugal acceleration

j—surfactant flux to the surface, eqn (13)

h—film thickness

h_{CR}—critical film thickness, at which the film spontaneously thins down and ruptures

h_{EQ}—equilibrium film thickness at given capillary pressure, Fig. 6C

h_{MIN}—minimal film thickness, Fig. 7C

k—numerical parameter in eqn (25) and (26)

k_B—Boltzmann constant

n_0—electrolyte concentration, in number of ions per unit volume

t—time

t_A—adsorption time, eqn (13)–(15)

t_C—collision time, eqn (11) and (12)

t_D—deformation time, eqn (7)–(10)

u—velocity

$\langle u^2 \rangle$—mean square fluctuations in the fluid velocity

Capital Greek letters

Φ—oil volume fraction

Γ—adsorption of the emulsifier on drop surface

Γ^*—threshold emulsifier adsorption required for obtaining stable emulsions (no electrostatic repulsions)

Γ_M—adsorption in a compelete monolayer

Π—disjoining pressure

Π_{EL}—electrostatic component of disjoining pressure, eqn (17) and (18)

Π_{VdW}—van der Waals component of disjoining pressure

Small Greek letters

α—three-phase contact angle of particle on fluid interface

β—parameter, eqn (31)

ε—rate of energy dissipation in the turbulent flow per unit mass of the fluid [J kg^{-1} s^{-1}]

ε_r—dielectric constant

$\dot{\gamma}$—shear rate during the emulsification experiments

ϕ_C—meniscus slope angle at the contact line of the particle, Fig. 7C

φ_{CP}—fraction of the surface area covered by adsorbed particles in complete monolayer

η—dynamic viscosity

η_C—viscosity of the continuous phase

η_D—viscosity of the dispersed phase

κ—Debye screening parameter

ψ_S—surface potential

θ^*—dimensionless threshold surface coverage, $\theta^* = \Gamma^*/\Gamma_M$

ρ—mass density

ρ_D—mass density of the dispersed phase

ρ_P—mass density of the particles

ρ_C—mass density of the continuous phase

$\Delta\rho = (\rho_C - \rho_D)$—mass density difference

σ—equilibrium interfacial tension

$\sigma(t)$—dynamic interfacial tension

Abbreviations

Brij, Brij 58-polyoxyethylene-20 hexadecyl ether

BLG—beta-globulin

CMC—critical micelle concentration of surfactant

IEP—isoelectric point

LMM surfactant—low-molecular- mass surfactant

PDMS—poly(dimethylsilaxane)

RCF—relative centrifugal acceleration, RCF = g_C/g

WPC—whey protein concentrate

Acknowledgements

The authors are grateful to Prof. I. B. Ivanov for the numerous useful discussions, to Dr K. Golemanov for some emulsification experiments, to Dr K. Marinova and Dr N. Vankova for the interfacial tension measurements (all from Sofia University, Bulgaria). This study was funded by Unilever R&D

Trumbull, CT, USA, and by the COST action P21 ''Physics of Droplets''.

References

1 B. P. Binks, *Curr. Opin. Colloid Interface Sci.*, 2002, **7**, 21.
2 R. Aveyard, B. P. Binks and J. H. Clint, *Adv. Colloid Interface Sci.*, 2003, **100–102**, 503.
3 B. P. Binks and T. S. Horozov, in *Colloidal Particles at Liquid Interfaces*, ed. B. P. Binks and T. S. Horozov, Cambridge University Press, Cambridge, 2006, pp. 1–76.
4 K. P. Velikov and O. D. Velev, in *Colloidal Particles at Liquid Interfaces*, ed. B. P. Binks and T. S. Horozov, Cambridge University Press, Cambridge, 2006, pp. 225–297.
5 Z. Du, M. P. Bilbao-Montoya, B. P. Binks, E. Dickenson, R. Ettelaie and B. S. Murray, *Langmuir*, 2003, **19**, 3106.
6 R. G. Alargova, D. S. Warhadpande, V. N. Paunov and O. D. Velev, *Langmuir*, 2004, **20**, 10371.
7 E. Dickinson, in *Colloidal Particles at Liquid Interfaces*, ed. B. P. Binks and T. S. Horozov, Cambridge University Press, Cambridge, 2006, pp. 298–327.
8 O. D. Velev, K. Furusawa and K. Nagayama, *Langmuir*, 1996, **12**, 2374.
9 O. D. Velev, K. Furusawa and K. Nagayama, *Langmuir*, 1996, **12**, 2385.
10 W. T. S. Huck, J. Tien and G. M. Whitesides, *J. Am. Chem. Soc.*, 1998, **120**, 8267.
11 A. D. Dinsmore, M. F. Hsu, M. G. Nikolaides, M. Marquez, A. R. Bausch and D. A. Weitz, *Science*, 2002, **298**, 1006.
12 V. N. Manoharan, M. T. Elsesser and D. J. Pine, *Science*, 2003, **301**, 483.
13 B. R. Midmore, *Colloids Surf., A*, 1998, **145**, 133.
14 B. P. Binks, J. H. Clint and C. P. Whitby, *Langmuir*, 2005, **21**, 5307.
15 J. Giermanska-Kahn, V. Laine, S. Arditty, V. Schmitt and F. Leal-Calderon, *Langmuir*, 2005, **21**, 4316.
16 S. Levine and B. D. Bowen, *Colloids Surf.*, 1991, **59**, 377.
17 S. Levine and B. D. Bowen, *Colloids Surf.*, 1992, **65**, 273.
18 S. Levine and B. D. Bowen, *Colloids Surf., A*, 1993, **70**, 33.
19 N. D. Denkov, I. B. Ivanov, P. A. Kralchevsky and D. T. Wasan, *J. Colloid Interface Sci.*, 1992, **150**, 589.
20 P. M. Kruglyakov and A. V. Nushtayeva, *Adv. Colloid Interface Sci.*, 2004, **108–109**, 151.
21 P. A. Kralchevsky and K. Nagayama, *Particles at Fluid Interfaces and Membranes: Attachment of Colloid Particles and Proteins to Interfaces and Formation of Two-Dimensional Arrays*, Elsevier, Amsterdam, 2001.
22 R. Aveyard, J. H. Clint and T. S. Horozov, *Phys. Chem. Chem. Phys.*, 2003, **5**, 2398.
23 R. Aveyard, J. H. Clint, D. Nees and V. N. Paunov, *Langmuir*, 2000, **16**, 1969.
24 R. Aveyard, J. H. Clint, D. Nees and N. Quirke, *Langmuir*, 2000, **16**, 8820.
25 W. Ramsden, *Proc. R. Soc. London*, 1903, **72**, 156.
26 S. U. Pickering, *J. Chem. Soc., Trans.*, 1907, **91**, 2001.
27 Th. V. Tadros and B. Vincent, in *Encyclopedia of Emulsion Technology*, ed. P. Becher, Dekker, New York, 1983, vol. 1, p. 129.
28 R. J. G. Lopetinsky, J. H. Masliyah and Z. Xu, in *Colloidal Particles at Liquid Interfaces*, ed. B. P. Binks and T. S. Horozov, Cambridge University Press, Cambridge, 2006, pp. 186–224.
29 B. P. Binks and S. O. Lumsdon, *Phys. Chem. Chem. Phys.*, 1999, **1**, 3007.
30 B. P. Binks and S. O. Lumsdon, *Langmuir*, 2000, **16**, 8622.
31 B. P. Binks and C. P. Whitby, *Langmuir*, 2004, **20**, 1130.
32 B. P. Binks and R. Murakami, *Nat. Mater.*, 2006, **5**, 865.
33 B. P. Binks and J. A. Rodrigues, *Angew. Chem., Int. Ed.*, 2005, **44**, 441.
34 S. Melle, M. Lask and G. G. Fuller, *Langmuir*, 2005, **21**, 2158.
35 B. P. Binks, R. Murakami, S. P. Armes and S. Fujii, *Angew. Chem., Int. Ed.*, 2005, **44**, 4795.
36 H. Xu, S. Melle, K. Golemanov and G. G. Fuller, *Langmuir*, 2005, **21**, 10016.
37 G. G. Fuller, E. J. Stancik and S. Melle, in *Colloidal Particles at Liquid Interfaces*, ed. B. P. Binks and T. S. Horozov, Cambridge University Press, Cambridge, 2006, pp. 169–187.
38 T. S. Horozov, R. Aveyard, J. H. Clint and B. P. Binks, *Langmuir*, 2003, **19**, 2822.
39 T. S. Horozov, R. Aveyard, J. H. Clint and B. Neumann, *Langmuir*, 2005, **21**, 2330.
40 P. A. Kralchevsky, I. B. Ivanov, K. P. Ananthapadmanabhan and A. Lips, *Langmuir*, 2005, **21**, 50.
41 S. Tcholakova, N. D. Denkov, I. B. Ivanov and B. Campbell, *Langmuir*, 2002, **18**, 8960.
42 S. Tcholakova, N. D. Denkov, D. Sidzhakova, I. B. Ivanov and B. Campbell, *Langmuir*, 2005, **21**, 4842.
43 S. Tcholakova, N. D. Denkov, D. Sidzhakova and B. Campbell, *Langmuir*, 2006, **22**, 6042.
44 K. Golemanov, S. Tcholakova, N. D. Denkov and Th. Gurkov, *Langmuir*, 2006, **22**, 3560.
45 K. Golemanov, S. Tcholakova, P. Kralchevsky, K. P. Ananthapadmanabhan and A. Lips, *Langmuir*, 2006, **22**, 4968.
46 S. Tcholakova, N. D. Denkov, I. B. Ivanov and B. Campbell, *Adv. Colloid Interface Sci.*, 2006, **123–126**, 259.
47 N. D. Denkov, S. Tcholakova and I. B. Ivanov, Globular proteins as emulsion stabilizers—similarities and differences with surfactants and solid particles, presented at the *4th World Congress on Emulsions*, Lyon, 2006.
48 S. Tcholakova, N. D. Denkov, D. Sidzhakova, I. B. Ivanov and B. Campbell, *Langmuir*, 2003, **19**, 5640.
49 S. Tcholakova, N. D. Denkov and T. Danner, *Langmuir*, 2004, **20**, 7444.
50 N. Vankova, S. Tcholakova, N. D. Denkov, V. Vulchev, I. B. Ivanov and T. Danner, *J. Colloid Interface Sci.*, 2007, **312**, 363.
51 N. Vankova, S. Tcholakova, N. D. Denkov, V. Vulchev and T. Danner, *J. Colloid Interface Sci.*, 2007, **313**, 612.
52 S. Tcholakova, N. Vankova, N. D. Denkov and T. Danner, *J. Colloid Interface Sci.*, 2007, **310**, 570.
53 P. Walstra, in *Encyclopedia of Emulsion Technology*, ed. P. Belcher, Marcel Dekker, New York, 1983, ch. 2.
54 C. A. Coulaloglou and L. L. Tavlarides, *Chem. Eng. Sci.*, 1977, **32**, 1289.
55 C. Tsouris and L. L. Tavlarides, *AIChE J.*, 1994, **40**, 395.
56 L. Taisne, P. Walstra and B. Cabane, *J. Colloid Interface Sci.*, 1996, **184**, 378.
57 S. Arditty, C. P. Whitby, B. P. Binks, V. Schmitt and F. Leal-Calderon, *Eur. Phys. J. E*, 2003, **11**, 273.
58 S. Arditty, V. Schmitt, J. Giermanska-Kahn and F. Leal-Calderon, *J. Colloid Interface Sci.*, 2004, **275**, 659.
59 A. N. Kolmogorov, *Dokl. Akad. Nauk SSSR*, 1949, **66**, 825 (in Russian).
60 J. O. Hinze, *AIChE J.*, 1955, **3**, 289.
61 F. B. Sprow, *Chem. Eng. Sci.*, 1967, **22**, 435.
62 J. T. Davies, *Chem. Eng. Sci.*, 1985, **40**, 839.
63 R. V. Calabrese, T. P. K. Chang and P. T. Dang, *AIChE J.*, 1986, **32**, 657.
64 C. Y. Wang and R. V. Calabrese, *AIChE J.*, 1986, **32**, 667.
65 P. D. Berkman and R. V. Calabrese, *AIChE J.*, 1988, **34**, 602.
66 C. Monteux, J. Kirkwood, H. Xu, E. Jung and G. G. Fuller, *Phys. Chem. Chem. Phys.*, 2007, **9**, 6344.
67 P. Walstra, in *Fundamentals of Interface and Colloid Science: Soft Colloids*, ed. J. Lyklema, Elsevier, Amsterdam, 2005, ch. 8.
68 V. G. Levich, *Physicochemical Hydrodynamics*, Prentice Hall, Englewood Cliffs, New Jersey, 1962.
69 V. Cristini, S. Guido, A. Alfani, J. Blawzdziewicz and M. Lowenberg, *J. Rheol.*, 2003, **47**, 1283.
70 A. K. Chesters, *Trans. Inst. Chem. Eng.*, 1991, **69**, 259.
71 T. D. Gurkov, S. C. Russev, K. D. Danov, I. B. Ivanov and B. Campbell, *Langmuir*, 2003, **19**, 7362.
72 T. D. Gurkov, D. T. Todorova, K. G. Marinova, C. Bilke-Crause, C. Gerber and I. B. Ivanov, *Colloids Surf., A*, 2005, **261**, 29.
73 R. Sedev, *Langmuir*, 2001, **17**, 562.
74 K. G. Marinova, R. G. Alargova, N. D. Denkov, O. D. Velev, D. N. Petsev, I. B. Ivanov and R. P. Borwankar, *Langmuir*, 1996, **12**, 2045.
75 B. V. Derjaguin, *Theory of Stability of Colloids and Thin Liquid Films*, Plenum Press, New York, 1989.

76 B. V. Derjaguin, N. V. Churaev and V. M. Muller, *Surface Forces*, Plenum Press, New York, 1987.
77 N. D. Denkov, *Langmuir*, 2004, **20**, 9463.
78 N. D. Denkov and K. G. Marinova, in *Colloidal Particles at Liquid Interfaces*, ed. B. P. Binks and T. S. Horozov, Cambridge University Press, Cambridge, 2006, pp. 383–444.
79 P. R. Garrett, in *Defoaming: Theory and Industrial Applications*, ed. P. R. Garrett, *Surf. Sci. Ser.*, Marcel Dekker, New York, 1993, vol. 45, ch. 1.
80 J. N. Israelachvili, *Intermolecular and Surface Forces*, Academic Press, New York, 1992.
81 W. B. Russel, D. A. Saville and W. R. Schowalter, *Colloidal Dispersions*, Cambridge University Press, Cambridge, 1989.
82 P. A. Kralchevsky, K. D. Danov and N. D. Denkov, in *Handbook of Surface and Colloid Chemistry*, ed. K. S. Birdi, CRC Press LLS, Boca Raton, 1997, ch. 11.
83 S. Mohan and G. Narsimhan, *J. Colloid Interface Sci.*, 1997, **192**, 1.
84 P. M. Adler, *J. Colloid Interface Sci.*, 1981, **84**, 461.
85 K. J. Ives, in *Solid–Liquid Separation*, ed. L. Svarovsky, Butterworths, London, 1981, ch. 4, part II.
86 S. Simovic and C. A. Prestidge, *Langmuir*, 2003, **19**, 3785.
87 S. Simovic and C. A. Prestidge, *Langmuir*, 2003, **19**, 8364.
88 C. A. Prestidge, T. Barnes and S. Simovic, *Adv. Colloid Interface Sci.*, 2004, **108–109**, 105.
89 B. P. Binks and S. O. Lumsdon, *Langmuir*, 2001, **17**, 4540.
90 B. P. Binks, R. Murakami, S. P. Armes, S. Fujii and A. Schmid, *Langmuir*, 2007, **23**, 8691.
91 B. P. Binks and J. A. Rodrigues, *Langmuir*, 2007, **23**, 7436.
92 G. Narsimhan and F. Uraizee, *Biotechnol. Prog.*, 1992, **8**, 187.
93 D. Cho, G. Narsimhan and E. I. Franses, *J. Colloid Interface Sci.*, 1997, **191**, 312.
94 K. D. Danov, D. S. Valkovska and P. A. Kralchevsky, *J. Colloid Interface Sci.*, 2002, **251**, 18.
95 I. B. Ivanov, K. P. Ananthapadmanabhan and A. Lips, *Adv. Colloid Interface Sci.*, 2006, **123–126**, 189.
96 N. G. van Kampen, *Stochastic Processes in Physics and Chemistry*, Elsevier, Amsterdam, 1981, ch. 11.
97 A. V. Nguyen and H. J. Schulze, *Colloidal Science of Flotation*, Marcel Dekker, New York, 2004.
98 A. V. Nguyen, R. J. Pugh and G. J. Jameson, in *Colloidal Particles at Liquid Interfaces*, ed. B. P. Binks and T. S. Horozov, Cambridge University Press, Cambridge, 2006, pp. 328–382.
99 K. D. Danov, P. A. Kralchevsky, K. P. Ananthapadmanabhan and A. Lips, *Langmuir*, 2006, **22**, 106.
100 Th. F. Tadros, *Applied Surfactants: Principles and Applications*, Wiley, WCH, 2006.
101 D. T. Wasan, in *Emulsions, Foams, and Thin Films*, ed. K.L. Mittal and P. Kumar, Marcel Dekker, 2000, pp. 1–35.
102 *Emulsions and Emulsion Stability*, ed. J. Sjoblom, *Surf. Sci. Ser.*, Marcel Dekker, 1996, vol. 61.
103 S. Tcholakova, N. D. Denkov, I. B. Ivanov and R. Marinov, *Bulg. J. Phys.*, 2004, **31**, 96.
104 G. A. van Aken and F. D. Zoet, *Langmuir*, 2000, **16**, 7131.
105 P. M. Kruglyakov, A. N. Nushtayeva and N. G. Vilkova, *J. Colloid Interface Sci.*, 2004, **276**, 465.
106 I. B. Ivanov, *Thin Liquid Films: Fundamentals and Applications*, Marcel Dekker, New York, 1988.
107 D. Exerowa and P. M. Kruglyakov, *Foams and Foam Films: Theory, Experiment, Application*, Elsevier, Amsterdam, 1998.
108 D. Exerowa, T. Kolarov and Khr. Khristov, *Colloids Surf.*, 1987, **22**, 171.
109 I. H. Black and T. M. Herrington, *J. Chem. Soc., Faraday Trans.*, 1995, **91**, 4251.
110 C. Stubenrauch and R. von Klitzing, *J. Phys.: Condens. Matter*, 2003, **15**, 1197.
111 V. Bergeron, A. Waltermo and P. M. Claesson, *Langmuir*, 1996, **12**, 1336.
112 E. D. Manev and R. J. Pugh, *Langmuir*, 1992, **7**, 2253.
113 J. Philip, G. Prakash, P. Kalyanasundaram, O. Mondain-Monval and B. Raj, *Langmuir*, 2002, **18**, 4625.
114 A. Waltermo, P. M. Claesson, S. Simonsson, E. Manev, I. Johansson and V. Bergeron, *Langmuir*, 1996, **12**, 5271.
115 R. Sedev and D. Exerowa, *Adv. Colloid Interface Sci.*, 1999, **83**, 111.
116 A. Scheludko, *Adv. Colloid Interface Sci.*, 1967, **1**, 391.
117 K. J. Mysels and M. N. Jones, *Discuss. Faraday Soc.*, 1966, **42**, 42.
118 G. Narsimhan, *Colloids Surf.*, 1992, **62**, 41.
119 G. Narsimhan and E. Ruckenstein, in *Foams*, ed. R. K. Prud'homme and S. A. Khan, *Surf. Sci. Ser.*, Marcel Dekker, New York, 1996, vol. 57, p. 99.
120 H. M. Princen, *Langmuir*, 1986, **2**, 519.
121 H. M. Princen, *Langmuir*, 1986, **3**, 36.
122 H. M. Princen, *Langmuir*, 1988, **4**, 164.
123 H. M. Princen, in *Encyclopedea of Emulsion Science and Technology*, ed. J. Soblom, Marcel Dekker, New York, 2001, ch. 11.
124 A. Vrij, *Discuss. Faraday Soc.*, 1966, **42**, 23.
125 I. B. Ivanov, B. Radoev, E. Manev and A. Scheludko, *Trans. Faraday Soc.*, 1970, **66**, 1262.
126 T. S. Horozov and B. P. Binks, *Angew. Chem., Int. Ed.*, 2006, **45**, 773.
127 N. D. Denkov, H. Yoshimura, K. Nagayama and T. Kouyama, *Phys. Rev. Lett.*, 1996, **76**, 2354.
128 N. D. Denkov, H. Yoshimura and K. Nagayama, *Ultramicroscopy*, 1996, **65**, 1.
129 K. P. Velikov, F. Durst and O. D. Velev, *Langmuir*, 1998, **14**, 1148.
130 E. J. Stancik, M. Kouhkan and G. G. Fuller, *Langmuir*, 2004, **20**, 90.
131 G. Mason and N. R. Morrow, *J. Colloid Interface Sci.*, 1994, **168**, 130.
132 E. Vignati and R. Piazza, *Langmuir*, 2003, **19**, 6650.
133 D. Stamou, C. Duschl and D. Johannsmann, *Rhys. Rev. E*, 2000, **62**, 5263.
134 P. A. Kralchevsky, N. D. Denkov and K. D. Danov, *Langmuir*, 2001, **17**, 7694.
135 N. D. Denkov, O. D. Velev, P. A. Kralchevsky, I. B. Ivanov, H. Yoshimura and K. Nagayama, *Langmuir*, 1992, **8**, 3183.
136 P. A. Kralchevsky and K. Nagayama, *Adv. Colloid Interface Sci.*, 2000, **85**, 145.
137 P. A. Kralchevsky and N. D. Denkov, *Curr. Opin. Colloid Interface Sci.*, 2001, **6**, 383.
138 N. D. Denkov, H. Yoshimura, T. Kouyama, J. Walz and K. Nagayama, *Biophys. J.*, 1998, **74**, 1409.
139 I. M. Lifshitz and V. V. Slyozov, *Zh. Eksp. Teor. Fiz.*, 1958, **35**, 479 (in Russian).
140 C. Wagner, *Electrochemistry*, 1961, **35**, 581.
141 A. S. Kabalnov, *Langmuir*, 1994, **10**, 680.
142 D. J. McClements and S. R. Dungan, *J. Phys. Chem.*, 1993, **97**, 7304.
143 A. S. Kabalnov and J. Weers, *Langmuir*, 1996, **12**, 3442.
144 J. Weiss, N. Herrmann and D. J. McClements, *Langmuir*, 1999, **15**, 6652.
145 J. Weiss, C. Canceliere and D. J. McClements, *Langmuir*, 2000, **16**, 6833.
146 Y. De Smet, L. Deriemaeker and R. Finsy, *Langmuir*, 1999, **15**, 6745.
147 S. Mun and D. J. McClements, *Langmuir*, 2006, **22**, 1551.
148 D. J. McClements, *Food emulsions: Principles, practice and techniques*, CRC Press, Boca Raton, 2004.
149 N. P. Ashby and B. P. Binks, *Phys. Chem. Chem. Phys.*, 2000, **2**, 5640.
150 M. Abkarian, A. B. Subramaniam, S. H. Kim, R. J. Larsen, S. M. Yang and H. A. Stone, *Phys. Rev. Lett.*, 2007, **99**, 188301.
151 S. I. Kam and W. R. Rossen, *J. Colloid Interface Sci.*, 1999, **213**, 329.
152 T. F. Svitova, M. J. Wetherbee and C. J. Radke, *J. Colloid Interface Sci.*, 2003, **261**, 170.
153 B. S. Murray, in *Proteins at Liquid Interfaces*, ed. D. Mobius and R. Miller, Elsevier, Amsterdam, 1998, ch. 5.
154 F. MacRitchie, in *Proteins at Liquid Interfaces*, ed. D. Mobius and R. Miller, Elsevier, Amsterdam, 1998, ch. 4.
155 V. N. Izmailova and G. P. Yampolskaya, *Adv. Colloid Interface Sci.*, 2000, **88**, 99.
156 G. Gonzalez and F. MacRitchie, *J. Colloid Interface Sci.*, 1970, **32**, 55.